Atmospheric and
Environmental Research, Inc.

Final Report on

Coupling Processes Between Atmospheric Chemistry and Climate (NAS5-97039)

Prepared by:

Malcolm Ko, Debra Weisenstein, Jose Rodriguez*, Michael Danilin, Courtney Scott, Run-Lie Shia, Janusz Eluszkiewicz, and Nien-Dak Sze

Atmospheric and Environmental Research, Inc.
840 Memorial Drive
Cambridge, MA 02139 USA

for

NASA Goddard Space Flight Center
Code 289
Greenbelt Road
Greenbelt, MD 20771

November, 1999

*Now at:
RSMAS/MAC
University of Miami
Miami, FL 33149

REPORT DOCUMENTATION PAGE

Form Approved
OMB No. 0704-0188

1. AGENCY USE ONLY *(Leave blank)*	2. REPORT DATE	3. REPORT TYPE AND DATES COVERED
	November 1999	Final Report; December 1996 - November 1999

4. TITLE AND SUBTITLE
Coupling Processes Between Atmospheric Chemistry and Climate

5. FUNDING NUMBERS
NAS5-97039

6. AUTHORS
M.K.W. Ko, Debra Weisenstein, Run-Li Shia and N.D. Sze

7. PERFORMING ORGANIZATION NAME(S) AND ADDRESS(ES)
Atmospheric and Environmental Research, Inc.
840 Memorial Drive
Cambridge, MA 02139

8. PERFORMING ORGANIZATION REPORT NUMBER
P698

9. SPONSORING/MONITORING AGENCY NAME(S) AND ADDRESS(ES)
NASA
Goddard Space Flight Center
Earth Sciences Procurement Office
Greenbelt, MD 20771

10. SPONSORING/MONITORING AGENCY REPORT NUMBER

11. SUPPLEMENTARY NOTES

12a. DISTRIBUTION/AVAILABILITY STATEMENT

12b. DISTRIBUTION CODE

13. ABSTRACT *(Maximum 200 words)*

This is the final report for NAS5-97039 for work performed between December 1996 and November 1999. The overall objective of this project is to improve the understanding of coupling processes among atmospheric chemistry, aerosol and climate, all important for quantitative assessments of global change. Among our priority are changes in ozone and stratospheric sulfate aerosol, with emphasis on how ozone in the lower stratosphere would respond to natural or anthropogenic changes.

The work emphasizes two important aspects:

(1) AER's continued participation in preparation of, and providing scientific input for, various scientific reports connected with assessment of stratospheric ozone and climate. These include participation in various model intercomparison exercises as well as preparation of national and international reports.

(2) Continued development of the AER three-wave interactive model to address how the transport circulation will change as ozone and the thermal properties of the atmosphere change, and assess how these new findings will affect our confidence in the ozone assessment results.

14. SUBJECT TERMS	15. NUMBER OF PAGES
	62
	16. PRICE CODE

17. SECURITY CLASSIFICATION OF REPORT	18. SECURITY CLASSIFICATION OF THIS PAGE	19. SECURITY CLASSIFICATION OF ABSTRACT	20. LIMITATION OF ABSTRACT
Unclassified	Unclassified	Unclassified	

Table of Contents

Appendices:

Abstract

This is the final report for NAS5-97039 for work performed between December 1996 and November 1999. The overall objective of this project is to improve the understanding of coupling processes among atmospheric chemistry, aerosol and climate, all important for quantitative assessments of global change. Among our priority are changes in ozone and stratospheric sulfate aerosol, with emphasis on how ozone in the lower stratosphere would respond to natural or anthropogenic changes.

The work emphasizes two important aspects:

(1) AER's continued participation in preparation of, and providing scientific input for, various scientific reports connected with assessment of stratospheric ozone and climate. These include participation in various model intercomparison exercises as well as preparation of national and international reports.

(2) Continued development of the AER three-wave interactive model to address how the transport circulation will change as ozone and the thermal properties of the atmosphere change, and assess how these new findings will affect our confidence in the ozone assessment results.

I. Updates to the 2-D Chemistry Transport Model

I.1 Refinements to the Formulation of the AER 2-D Chemistry Transport Model and Sulfate Model

The AER 2-D chemical-transport model (CTM) has been maintained and enhanced under this contract so that credible assessments of ozone could be performed. The chemical reaction rates were updated in 1997 to remain current with the JPL recommendations (DeMore et al., 1997). Another major upgrade performed in 1997 affects how temperatures are used to calculate reaction rates. In previous versions of the AER 2-D model, temperature-dependent reaction rate constants were computed using $k(<T(\theta,z,t)>)$, where $<T(\theta,z,t)>$ is the zonal-mean temperature at latitude θ, altitude z, and time of the year t obtained by interpolating monthly zonal-mean temperature files. To account for the effect of longitudinal and temporal variations in temperature on photochemical reaction rates, monthly zonal mean temperature statistics were compiled for the 1979-1995 period based on data from the NCEP/NCAR reanalysis project (Kalnay et al., 1996). Probability distribution functions, $P_{(\theta,z,t)}(T)$, defined to represent the probability of encountering the temperature T at latitude θ, altitude z, during the month M were created by combining daily data for each month and in each zonal band for the 17-year period. These distributions were found to be much broader in winter than in summer at mid and high latitudes. Temperature-dependent reaction rates are now calculated in the model by integrating the product of the rate and temperature probability for each 1 K of the distribution:

$$< k_{eff} > (\theta, z, t) = \int_0^\infty k(T) P_{(\theta,z,M)}(T) dT.$$

$<k_{eff}>(\theta,z,t)$ is now used in the photochemistry calculation instead of $k(<T(\theta,z,t)>)$. The rates which are most sensitive to temperature variations are the heterogeneous reactions such as $ClNO_3$+HCl and HOCl+HCl that occur on sulfate aerosols.

A parameterization for calculating the surface area of type I and type II polar stratospheric clouds (PSCs) was added to the AER 2-D model. The parameterization is based on equilibrium vapor pressure calculations rather than microphysics and is independent of the sulfate aerosol density. The local temperature determines the equilibrium vapor concentration of HNO_3 and H_2O. Excess HNO_3 and H_2O are assumed to form nitric acid trihydrate (NAT) particles. At lower temperatures, excess water condenses to form ice particles. The thermodynamic equilibrium calculation assumed no supersaturation requirement, but this can be easily modified. PSC particles are assumed monodispersed in size, with NAT particles of 0.5 μm radius and ice particles of 7 μm radius. In order to calculate realistic PSC surface area densities and reaction rates in the 2-D model, the temperature probability distribution is applied

such that we calculate a NAT and ice surface area, $A(T)$, at each temperature in the distribution, multiply by the temperature-dependent heterogeneous reaction rate, $\gamma(T)v(T)/4$, and the probability of occurrence of that temperature, and sum over the distribution:

$$< k_{het-eff} > (\theta, z, t) = \int_0^\infty \tfrac{1}{4}\gamma(T)v(T)A(T)P_{(\theta,z,M)}(T)dT.$$

The grid resolution of the AER 2-D model is somewhat flexible, but the transport circulation most often used is for a grid resolution of 9.5° latitude by 1.2 km in the vertical. We have recently upgraded the model to easily handle increased horizontal resolution. A resolution of 5° latitude by 1.2 km in the vertical has been chosen for future work and will be used when creating new transport circulations. The 5° horizontal resolution will allow for better representation of the polar vortex edge and thus better treatment of polar chemistry and PSCs. Several transport circulations have already been created with the enhanced horizontal resolution and are discussed below.

The AER 2-D sulfate aerosol model (Rinsland et al., 1995; Weisenstein et al., 1997) was developed for assessment of the impact on ozone of volcanic eruptions and aircraft emission of sulfur. The concentrations of sulfur-bearing species CS_2, H_2S, DMS, MSA, OCS, SO_2, SO_3, and H_2SO_4 are calculated as in the 2-D CTM. Aerosol microphysics for binary sulfuric acid-water particles in 40 size bins, ranging from 0.4 nm to 3.2 μm radius by volume doubling, is also included. Gas phase H_2SO_4 is converted to aerosol particles via homogeneous nucleation (Yue and Deepak, 1982), which creates new aerosol particles, and condensation (Hamill and Yue, 1979), which increases the size of existing aerosol particles. The nucleation scheme was upgraded to that of Zhao and Turco (1995) which results in greater accuracy with less computer time. Because of the extreme sensitivity of homogeneous nucleation rates to temperature, the temperature probability distribution is employed to account for deviations from the zonal mean temperature in the calculation of nucleation rates. Evaporation of aerosols in the upper stratosphere converts liquid sulfuric acid back to gas phase. Coagulation (Yue and Deepak, 1979) decreases the aerosol number density while maintaining total aerosol volume. Aerosol composition (i.e., weight percent of sulfuric acid) is calculated interactively based on ambient water vapor and temperature, originally using the formula given by Steele and Hamill (1981), but recently upgraded to the formula of Tabazadeh et al. (1997). Evaporation/condensation of H_2O onto aerosols is assumed to occur instantaneously to maintain the equilibrium composition. Each size bin is transported separately by the model's residual mean circulation, with the appropriate sedimentation rate (Kasten, 1968) applied. Sedimentation leads to a redistribution of the larger

particles, which fall faster at higher altitudes. Aerosols are removed in the troposphere by washout and dry deposition.

The AER 2-D sulfate aerosol model was developed using the framework of the AER 2-D chemistry-transport model, but was set up as a separate model. It used the same grid, advection algorithm, and transport circulation, as well as the same methodology for the chemical scheme. But the only species modeled were the sulfur-containing compounds and sulfate aerosols. Other species which interact with sulfur species, such as OH, O, and O_3, were assumed to be unaffected by changes in sulfur-containing species or aerosols. These species were taken from a previous calculation of the AER 2-D chemistry-transport model. This assumption was a reasonable approximation and allowed for more rapid development of the sulfate aerosol model. However, having a model which calculates sulfate aerosols and also the full suite of chemicals controlling ozone would allow for more feedbacks and simplify scenario calculations. It would also allow for interaction of sulfate aerosols and PSC in the winter polar regions by allowing condensation of HNO_3 on sulfate aerosols. Work towards combining the sulfate and chemistry-transport models was begun in December 1998. First the code dealing with aerosols was isolated into 2 interface routines which could be called from the chemistry-transport model. Then common blocks were synchronized between the two models and some modifications made to facilitate interaction. Finally, the chemical species and reactions of the sulfate model were added to the chemistry-transport model. The aerosol routines are called during model calculations only if the variable "LAERO" is set to true in the setup file. If aerosols are not calculated during the model run, the WMO background aerosol surface area density (SAD) is used in the calculation of heterogeneous chemistry. In addition, aerosol SAD may be specified from a file as a function of latitude, altitude, and season.

The combined sulfate/chemistry 2-D model has been functional since mid-June, 1999. Calculations have been performed for 1992 conditions at both 9.5° and 5° horizontal resolution, with chemical species and aerosol densities similar to those obtained from the separate models. Aerosols currently interact with the full suite of trace gases in the following respects: calculated ozone is used to calculate photolysis rates which control dissociation of sulfur-bearing compounds; OH can be modified by interaction with sulfur-bearing compounds, though this should be significant only following very large volcanic eruptions; and the calculated sulfate aerosol SAD determines the rate of heterogeneous reactions on sulfate aerosol, which control the concentration of O_3 and the partitioning of the NO_y, Cl_y, and Br_y species. Still to be implemented is use of the full aerosol size distribution in the calculation of heterogeneous rates for $ClNO_3$+H_2O, $ClNO_3$+HCl, HOCl+HCl, and HOBr+HCl which depend on aerosol volume. We also plan to update our PSC scheme so that sulfate aerosols and PSC particles can interact, probably though implementation of an STS scheme which allows for condensation of HNO_3 and

additional H_2O on existing sulfate aerosols, modifying the composition, size, and reactivity of the particles.

I.2 Improvements to the Transport Circulation in the AER 2-D Model

I.2a Transport Across the Subtropical Barrier

The correct representation in a 2-D CTM of the transport in the lower stratosphere, especially the mixing between the tropics and the middle latitudes, are important for simulating the stratospheric ozone and other species important to the global change investigation. Most anthropogenic pollution emitted at the earth surface enters the stratosphere through the tropics. Therefore, the mixing across the tropical barrier governs how much of the pollution would enter the extratropics of the lower stratosphere and how much of it goes up to the upper stratosphere, where it is more likely to be destroyed photochemically. We have shown that the mixing rate in a 2-D CTM is controlled solely by the horizontal eddy diffusion coefficients, K_{yy} (Shia et al., 1998, ***Appendix A***). This allows us to use the exchange rates between the tropics and mid-latitudes, if known, to adjust K_{yy} in AER 2-D CTM to simulate the tropical barrier.

In situ measurements of chemical species with a wide range of local lifetimes have been used to quantify the air exchange rate between the tropics and mid-latitudes in the lower stratosphere from the tropopause to around 21 km. It is found that the mid-latitude air is entrained into the tropical lower stratosphere with a replacement time scale of 10-18 months (Minschwaner et al., 1996; Volk et al., 1996). Meanwhile, Schoeberl et al. (1997) estimate the mixing time between the tropics and mid-latitudes in the 20-28 km region to be at least 18 months using the QBO signals in the N_2O/CH_4 ratio and tropical winds from UARS measurements. These results demonstrate that the tropical barrier allows a moderate penetration (i.e., a leaky pipe).

The tropical barrier (leaky pipe) is simulated in the AER 2-D CTM by assigning proper values of K_{yy} in the tropical lower stratosphere to produce correct exchange rates. The horizontal diffusion fluxes and mixing ratios of CCl_4, CF_2Cl_2, $CFCl_3$, CH_3CCl_3, CH_4, HNO_3, N_2O, NO_y, and O_3 calculated in the model are used to derive the exchange rates between the tropical and mid-latitude lower stratosphere. With a K_{yy} of 0.3 x 10^6 m^2/sec, which was used in early versions of AER 2-D global diffuser model, the exchange rate is calculated to be about 5-6 months. When a tropical pipe is included in the model by reducing the values for K_{yy} to 0.03 x 10^6 m^2/sec (Weisenstein et al., 1996), the model results show a much slower exchange rate of 38-60 months. A new set of values between 0.03-0.3 x 10^6 m^2/sec for K_{yy} are chosen to generate exchange rates of around 14 months below 20 km and 18 months in the 20-30 km region. These values of exchange rates are similar to those estimated from measurements.

Even though the changes of K_{yy} are limited to a small area in the tropical lower stratosphere, they are significant in determining the lifetimes of long-lived source gases. For some species, the adjustment in K_{yy} generated a change in calculated lifetime of more than 10%. In assessing the atmospheric effects of the future high speed aircraft, adjusting K_{yy} can produce a change in global ozone depletion of more than 20% (1.24 D.U. calculated by the global diffuser model, 0.8 D.U. by the tropical pipe model and 0.99 D.U. by the leaky pipe model). The effect of the subtropical barrier reduces the transport of the HSCT engine emissions across the tropics into the southern hemisphere, thus significantly reducing calculated ozone depletion there. The uncertainty in HSCT assessment due to transport can have the same order of magnitude as other major uncertainties, such as those due to uncertainties in the HSCT aircraft emission budget or in atmospheric photochemistry. Detailed results of this study can be found in Shia et al. (1998), ***Appendix A***.

I.2b Transport Across the Polar Barrier

The results of the Models and Measurements II experiments showed that there are significant defects in the transport parameters currently used in most 2-D chemistry transport models. One of these defects is the lack of a clear polar vortex. Large numbers of observations and measurements show that the fast isentropic mixing created by planetary wave breaking cannot penetrate into the polar vortex and the concentrations of long-lived species, e.g. N_2O and CH_4, have strong gradients across the polar vortex wall. This feature is not seen in the results of the AER 2-D CTM (Figure I.1a). In the model, the isentropic mixing is represented by the eddy diffusion coefficient, K_{yy}. Smaller values of K_{yy} should be assigned at the polar barrier to simulate the vortex. The measurements of long-lived species by instruments aboard UARS, with nearly global coverage and high precision, provide a useful database for adjusting K_{yy} across the polar vortex. Recently, Randel et al. (1998) processed the UARS/MLS and UARS/CLAES CH_4 data to create distributions of CH_4 on an altitude-equivalent latitude grid by averaging the data along potential vorticity (PV) contours to avoid smoothing the tracer gradients across the vortex edge. These new 2-D distributions of CH_4 reveal the polar barriers, which greatly reduce the mixing between the mid-latitudes and polar region (Figure I.1b).

We have used these CH_4 distributions to adjust the mixing across the polar vortex in the AER 2-D CTM. We define a cost function to measure the difference between the gradients of CH_4 on the polar vortex edge from the model simulations and from Randel's data. By adjusting the K_{yy} to minimizing the cost function, we derive values for K_{yy} near the polar vortex. Using the values of K_{yy} which produce the minimum cost function significantly improves the model

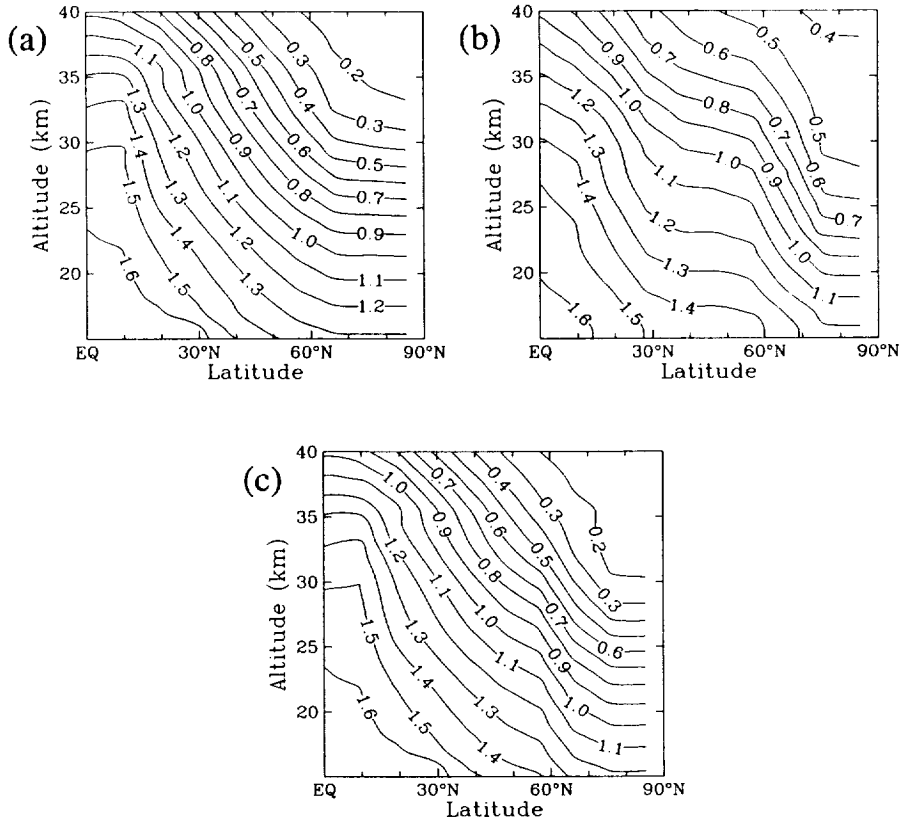

Figure I.1 Latitude-altitude distribution of CH_4 mixing ratio (ppmv) in the northern hemisphere for February (a) as simulated by the AER 2-D CTM, (b) from UARS observations (Randall et al., 1998), and (c) as simulated by the AER 2-D CTM with polar barrier.

simulation of CH_4 across the polar barrier (Figure I.1c). These adjusted values of K_{yy} for both northern and southern polar vortices were used in the 2-D CTM with detailed photochemistry to calculate many long-lived species concentrations. The new version of the full 2-D model improves the simulation of these species in the polar region. Unlike in the subtropical barrier case, the adjustment of K_{yy} in the polar barrier only has localized effects on the age of air calculation and the simulated atmospheric effects of the High Speed Civil Transport (HSCT). The exchange time scale between the polar vortex and the middle latitudes is calculated using the same method as for the subtropical barrier (Shia et al., 1998). This study was presented at the 1998 AGU Fall Meeting and is reproduced here as ***Appendix B***.

I.2c Use of Different Transport Circulations in the AER 2-D Model

We have made use of the flexibility of the AER 2-D CTM by running the model with different transport circulations at different grid resolutions. An intercomparison study was performed between the AER, GSFC, and LLNL 2-D models (Weisenstein et al., 1998) in which the transport formulations of those models were run within the AER model at their native grid

resolutions. An inert tracer calculation with source similar to HSCT-emitted NO_y was run to confirm that the transport was implemented properly. Small differences (4-6% above 20 km, larger near tropopause) were found between the AER model running the GSFC circulation and the GSFC model itself due to the different transport schemes used (Lin and Rood for GSFC, Smolarkiewicz for AER). We obtained a good match (within 3% everywhere) with the LLNL model, as these models use the same transport scheme. Comparisons between versions of the AER model running different transports can be used to assess model sensitivity to transport. Comparisons of different models running the same transports are used to assess differences in chemical formulation, which includes the family grouping technique, the diurnal averaging technique, and the polar chemistry parameterization. Differences in NO_y (up to 7%) were found between models with the same circulation, most likely due to differences in the calculated upper stratospheric loss for this species. The PSC treatment differed among the three models studied, and so ozone was quite different at high latitudes. An HSCT perturbation calculation also found sensitivities to the model chemical formulation, especially in the polar latitudes. This study was presented at the 1998 AEAP meeting and is reproduced here as ***Appendix C***.

In an effort to improve the transport circulation of the AER 2-D model, several new streamfunctions have been generated on a 5° latitude by 1.2 km vertical resolution grid utilizing diabatic heating rates derived from UARS and NCEP. Three different sets of radiative heating rates have been derived from UARS data, based on ozone, temperature, and water vapor measurements from MLS (version 3) for 1992 and 1993, and from CLAES (version 17) for 1992 (supplemented in all cases by climatological fields below 100 mb). The UARS-based calculations of the heating rates are described in Eluszkiewicz et al. (1996, 1997). The NCEP diabatic heating rates are from the reanalysis climatology for the period 1982 to 1994 (Kalnay et al., 1996). These model-generated fields include contributions from radiative heating, large-scale condensation, deep convection, shallow convection, and vertical diffusion. The nonradiative NCEP heating rates have also been used with the UARS-based radiative heating rates to generate fields of total diabatic heating. We do not have diffusion fields which are consistent with these advective circulations. Therefore we have experimented with using the standard AER diffusion fields (the leaky pipe formulation described above), the GSFC model diffusion fields which were calculated to be consistent with the GSFC advective field (Jackman et al., 1996; Fleming et al., 1999), and other combinations. Model calculations with these alternate transport formulations are described in Section VII of this report, where sensitivity studies and age of air calculations are shown.

II. Chlorine and Bromine Loading in the Stratosphere

II.1 On the Relation Between Stratospheric Chlorine/Bromine Loading and Short-lived Tropospheric Source Gases

Current methods for estimating the concentrations of inorganic chlorine/bromine species (Cl_y/Br_y) in the stratosphere due to decomposition of tropospheric source gases assume that the Cl_y/Br_y concentration in the stratosphere is determined mainly by the balance between production from *in situ* oxidation of the source gases in the stratosphere and removal by transport of Cl_y/Br_y out of the stratosphere. The rationale being that, for source gases whose lifetime is of order several months or longer, the concentration of Cl_y/Br_y in the troposphere is small because they are produced at a relatively slow rate and removed efficiently by washout processes. As a result of the small concentration, the rate at which Cl_y/Br_y are transported to the stratosphere is expected to be small compared to the *in situ* stratospheric production. Thus, the transport of Cl_y/Br_y from the troposphere contributes little to the stratospheric concentration. In contrast, the origin of stratospheric Cl_y/Br_y from reactive source gases with tropospheric lifetimes comparable to the washout lifetime of Cl_y/Br_y (of order 10-30 days) in the troposphere is distinctly different. The *in situ* source in the stratosphere is expected to be significantly smaller because only a small portion of the source gas is expected to survive the troposphere to be transported into this region. At the same time, these short-lived source gases produce appreciable amounts of Cl_y/Br_y in the troposphere such that transport to the stratosphere offers a larger source for stratospheric Cl_y/Br_y than *in situ* production. Thus, for reactive source species, simple methods of estimating the concentration of stratospheric Cl_y/Br_y that ignore the tropospheric contribution will seriously underestimate the loading. Therefore, estimation of the stratospheric Cl_y/Br_y loading requires not only measurements of tropospheric source gases but also measurements of Cl_y/Br_y at the tropopause. We have further examined this mechanism by using results from a two-dimensional chemistry-transport model. However, in view of the importance of tropospheric transport on stratospheric loading, the detailed values should be further evaluated using a three-dimensional model with appropriate treatment of convective transport.

The results of this study were published in JGR. A reprint is included as ***Appendix D.***

II.2 Distribution of Halon-1211 in the Upper Troposphere and Lower Stratosphere and the 1994 Total Bromine Budget

Stratospheric air was analyzed with a new gas chromatograph, flown aboard the NASA ER-2 aircraft as part of the Airborne Southern Hemisphere Ozone Experiment/Measurements for Assessing the Effects of Stratospheric Aircraft mission conducted in 1994. The mixing ratio of

SF_6, with its nearly linear increase in the troposphere, was used to estimate the mean age of stratospheric air parcels along the ER2 flight path. Measurement of H-1211 and mean age estimates were then combined with simultaneous measurements of CFC-11, measurements of brominated compounds in stratospheric whole air samples, and records of tropospheric organic bromine mixing ratios to calculate the dry mixing ratio of total bromine in the lower stratosphere and its partitioning between organic and inorganic forms. We estimate that the organic bromine-containing species were almost completely photolyzed to inorganic species in the oldest air parcels sampled. Our results for inorganic bromine are consistent with those obtained from a photochemical, steady state model for stratospheric air parcels with CFC-11 mixing ratios greater than 150 ppt. For stratospheric air parcels with CFC-11 mixing ratios less than 50 ppt (mean age $\geq$ 5 years) we calculate inorganic bromine mixing ratios that are approximately 20% less than the photochemical steady state model. There is a 20% reduction in calculated ozone loss resulting from bromine chemistry in old air relative to some previous estimates as a result of the lower bromine.

The results of this study were published in JGR. A copy of the reprint is included as ***Appendix E.***

III. Model Analysis of the Nitrogen Species Partitioning in the Stratosphere

Nitrogen species play an important role for the photochemical ozone balance in the atmosphere (e.g., WMO, 1995, 1999; Wennberg, 1994). Testing abilities of the photochemical models to reproduce partitioning of the nitrogen species partitioning between short-lived radicals NO and NO_2 (called usually as NO_x) and a relatively long-lived reservoir HNO_3 is important for understanding of the impacts produced by the current and future anthropogenic NO_x emissions. Also, predictive capabilities of the assessment models should be tested against available measurements since the composition of the future atmosphere is expected to change due to reduction of the chlorine species in the atmosphere and cooling of the stratosphere. Additionally, direct comparison of the properly constrained model results against measurements could be useful for analysis of the existing kinetics data or prediction of new unknown reactions.

During this project we have compared model calculations of the nitrogen species versus *in situ* (balloon) and remote (satellite) measurements. Comparison of the model calculations and balloon measurements is discussed in Section III.1.

It is well established that the partitioning of the nitrogen species is sensitive to the aerosol loading of the stratosphere (e.g., Rodriguez et al., 1991; Fahey et al., 1993) due to the following rapid heterogeneous reactions:

$$N_2O_5 + H_2O \rightarrow HNO_3 + HNO_3 \qquad \text{(R1)}$$

$$BrONO_2 + H_2O \rightarrow HOBr + HNO_3 \qquad \text{(R2)}$$

To analyze the behavior of nitrogen species after the Pinatubo eruption, the strongest in this century, we looked at the near-global UARS measurements and AER box model calculations (Danilin et al., 1999) in Section III.2.

III.1 Model Analysis of the Balloon Measurements

Balloon measurements have a very good vertical resolution and provide quite accurate data of radicals and tracers in the atmosphere. They are attractive for the model analysis, since several key species and atmospheric parameters (like temperature and aerosol concentration) are measured simultaneously placing (depending on the payload) good constraints on the model calculations.

Since, at the moment that this report was written, the Kondo et al. (1999) paper is still in press, we give some details of this study. The balloon measurements of NO, HNO_3, NO_y, N_2O, O_3, and aerosol were made from Aire sur l'Adour (France, 44°N, 0°W) on October 12, 1994.

Detailed descriptions of the NO and NO_y chemiluminescence detectors are given in Kondo et al. (1997). We picked this flight for our analysis, since additionally nitric acid was measured by a mass spectrometer, thus providing good constraints for the model analysis of the nitrogen species partitioning. Another reason for model analysis of this particular flight was the fact that aerosol loading of the stratosphere was approaching its background values, since more than 3 years passed after the Pinatubo eruption. Since the global atmosphere spends most of its time near the background conditions and powerful volcanic eruptions happen rather rarely, consistency of the model calculations and measurements under such conditions is crucial for our understanding of the stratospheric photochemistry.

Figure III.1 shows the vertical distribution of NO, HNO_3, and NO_y during this flight. Model analysis of these measurements is performed by the GSFC (Kawa et al., 1993) and AER (Danilin et al., 1998) trajectory models.

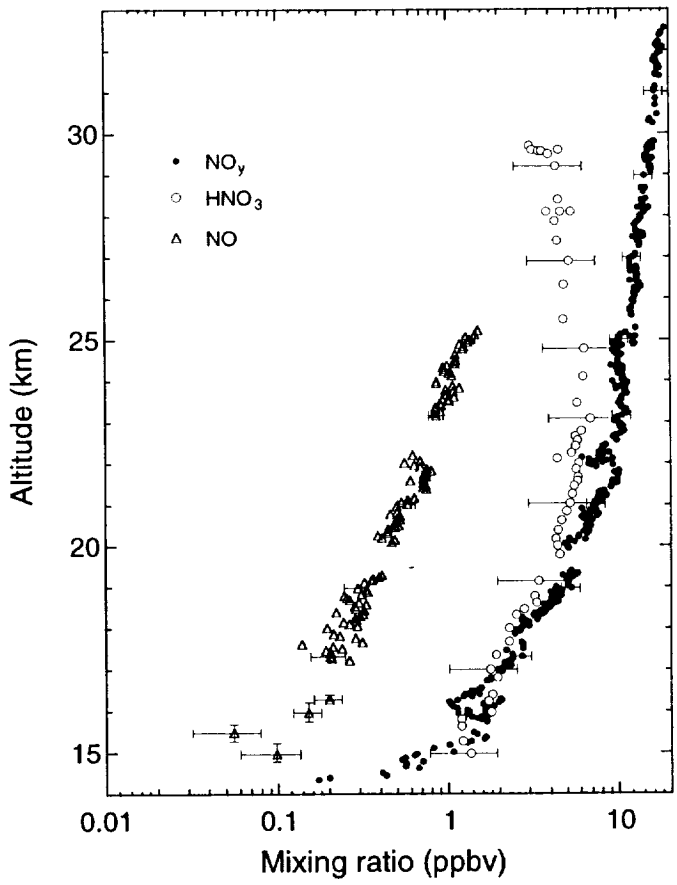

Figure III.1 Vertical profiles of the NO (open triangles), NO_y (closed circles), and HNO_3 (open circles) mixing ratios observed on October 12, 1994. The +/-1 sigma standard deviations over the intervals are shown as bars.

Since their results are practically coincident (within 10%), the averaged (i.e. (GSFC+ AER)/2) model curves are shown in Figure III.2. The NO/NO_y ratio is a good indicator of the partitioning between radical and total nitrogen species. Our results show that only gas-phase chemistry considerably overestimates the NO/NO_y ratio and could not explain the measurements, thus confirming the role of the reactions (R1) and (R2) for the nitrogen species partitioning. On the other hand, inclusion of heterogeneous reactions (R1)-(R2) on sulfate aerosol with the gas-phase kinetics according to the JPL-97 recommendations (DeMore et al., 1997) underestimates the NO/NO_y ratio. However, when the updated reaction rates for the $OH + NO_2 + M \rightarrow HNO_3 + M$ (Brown et al., 1999a) and $HNO_3 + OH \rightarrow NO_3 + H_2O$ (Brown et al., 1999b) are used, a much better agreement between model and measurements is obtained. Thus, this study confirms important implications of new rates of these reactions for the stratospheric photochemistry. More details are presented in Kondo et al. (1999).

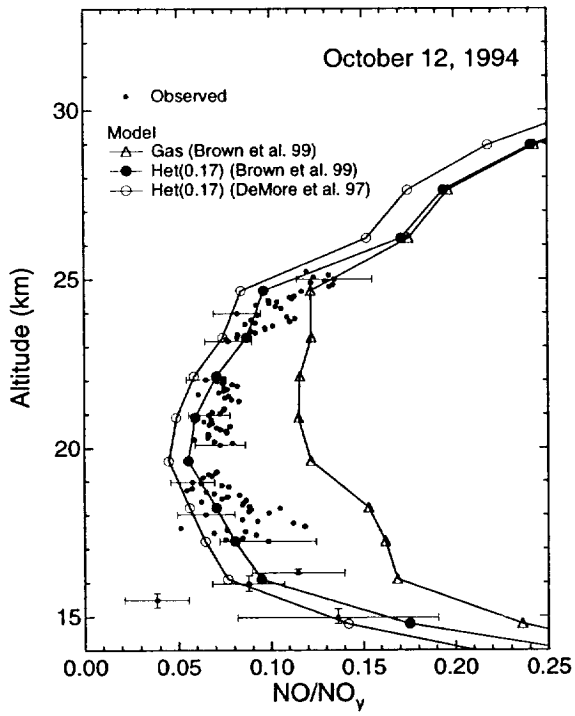

Figure III.2 Vertical profiles of the NO/NO_y ratios observed by the balloon (black circles) and calculated by the GSFC and AER models (the AER+GSFC/2 results are shown). Open triangles correspond to the model results without heterogeneous reactions on sulfate aerosol, but with the new reaction rates for the (R1)-(R2) reactions according to Brown et al (1999a,b). The model calculations with the (R1)-(R2) heterogeneous reactions using SAD from the balloon aerosol channel measuring particles with diameter less than 0.17 microns and applying the JPL-97 and Brown et al. (1999a,b) recommendations for the $OH + NO_2$ and $HONO_3 + OH$ reactions are shown by the open and closed circles, respectively.

III.2 Model Analysis of the Satellite Measurements

A big advantage of the satellite versus balloon measurements is a much larger spatial and temporal coverage. For example, the Upper Atmosphere Research Satellite (UARS) covers the 80°S-80°N latitude band and some instruments on its board provide almost uninterrupted data sets from the end of 1991 up to now (e.g., HALogen Occultation Experiment (HALOE)). Since the UARS was launched about 3 months after the Mt. Pinatubo eruption, there was a unique opportunity to analyze the response of the atmosphere to this strong volcanic perturbation.

We utilize UARS data to investigate whether the observed NO_x/NO_y, NO, NO_2, and HNO_3 distributions under the wide range of aerosol loading conditions found in the post-Pinatubo stratosphere are consistent with those predicted by our model calculations. We created the merged yearly and monthly averaged files of the following measured species: HALOE v.18 CH_4, NO, NO_2, H_2O, O_3, HCl; and CLAES v.7. N_2O, HNO_3, $ClONO_2$, and N_2O_5 (for details see Danilin et al. (1999)). The steady-state version of the AER box model constrained by the HALOE O_3, CH_4, and H_2O and SAGE-II aerosol surface area density was applied for our analysis. Since total nitrogen NO_y was not measured by the UARS, three different initializations of NO_y were applied: 1) NO_y as a sum of the measured NO, NO_2, HNO_3, and $ClONO_2$; 2) NO_y from the NO_y-N_2O correlation using CLAES N_2O measurements; and 3) NO_y from the NO_y-CH_4 correlation using HALOE CH_4 measurements.

Our sensitivity study has shown that the NO_x/NO_y ratio is not sensitive to the absolute values of NO_y, thus model calculated NO_x/NO_y are practically the same for all initializations of NO_y used. Figure III.3 shows the comparison of the model calculated and the UARS measured sunset NO_x/NO_y ratio for the January 1992 to September 1994 period. Our model reproduces reasonably well the seasonal evolution and altitudinal dependence of the NO_x/NO_y ratio. However, the model tends to underestimate the NO_x/NO_y ratio at 31 and 22 mb at 45°N and 45°S.

Figure III.4 investigates in detail the altitudinal-latitudinal dependence of the NO_x/NO_y ratio in January 1993. Despite a good agreement between model calculations with heterogeneous chemistry (red lines) and measurements at 68 and 46 mbar, the model tends to underestimate the fraction of the reactive nitrogen from 31 mb to 10 mb. Reduction of the OH + NO_2 + M $\rightarrow$ HNO_3 + M reaction rate by 25% (grey lines) makes model calculations closer to the measurements, however does not solve this problem.

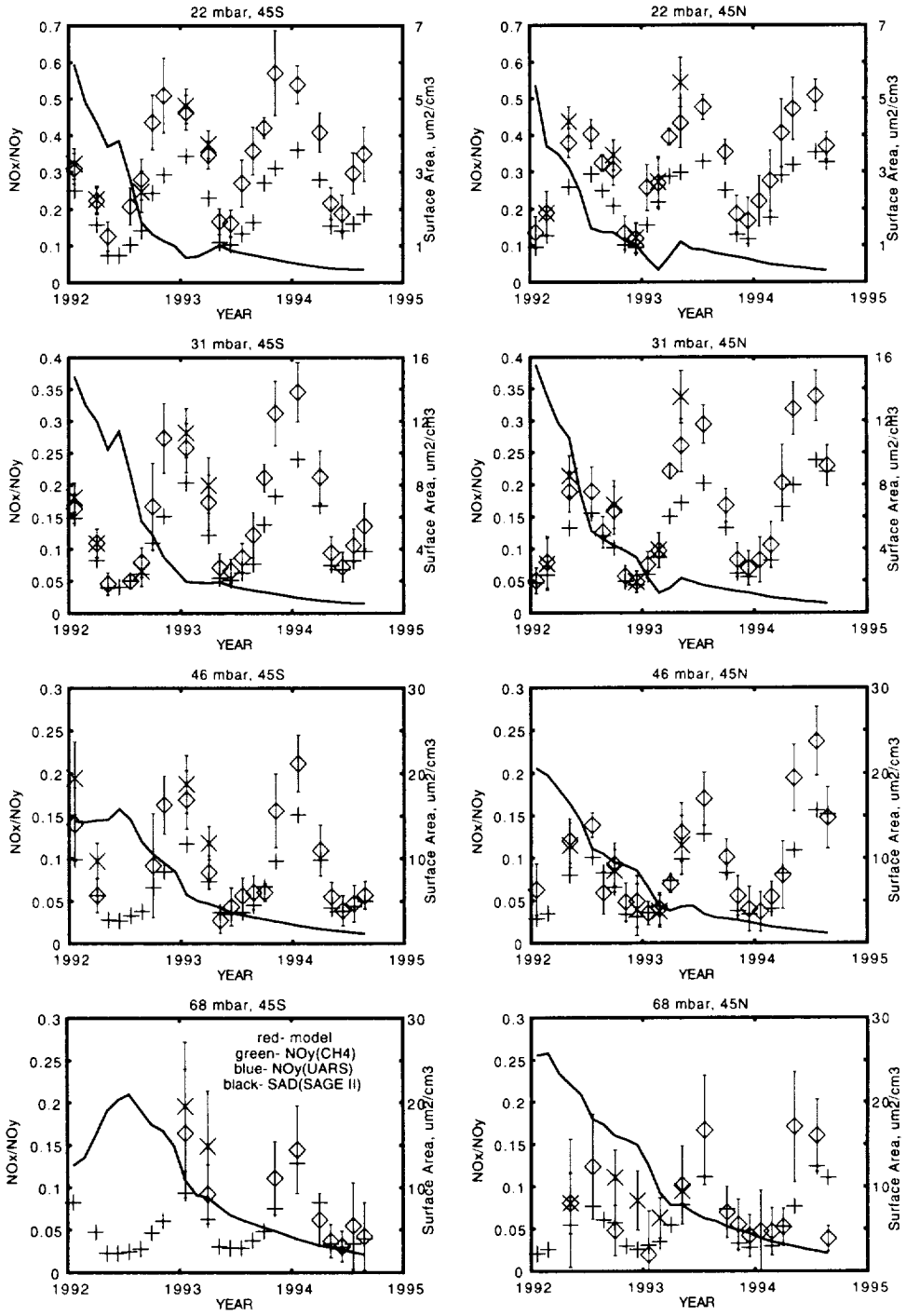

Figure III.3 Temporal evolution of the sunset NO_x/NO_y ratio from January 1992 to September 1994 at 45°S (left column) and 45°N (right column) at the 68-, 46-, 32-, and 22-mbar levels. Green and blue symbols with error bars correspond to the UARS data with NO_y according to the CH_4 and UARS initializations, respectively; red crosses indicate box model calculations. The N_2O and UARS approaches can provide NO_y data only until May 1993 because of the CLAES lifetime. The black lines show behavior of aerosol surface area density (right vertical axis, in micron^2/cm^3).

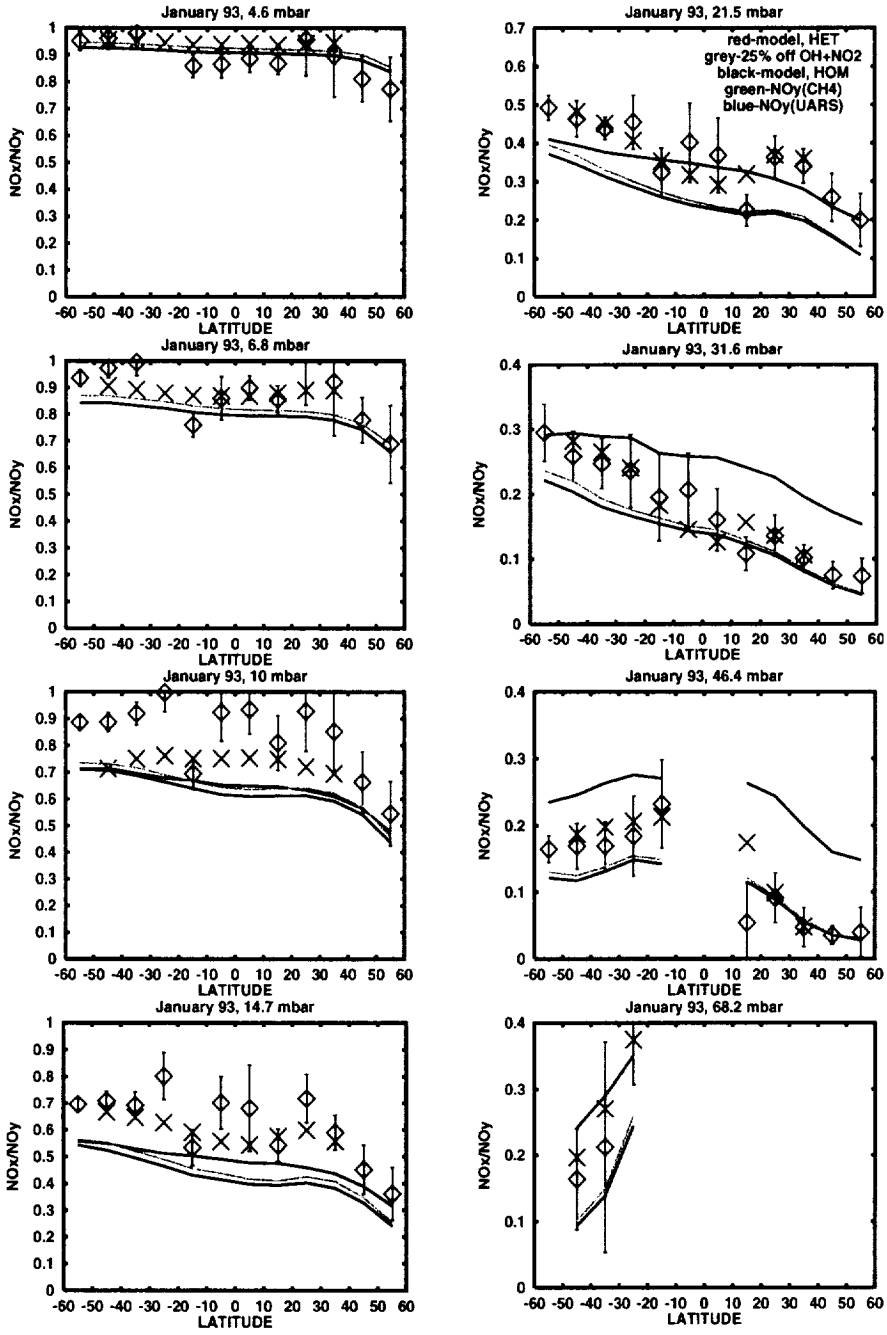

Figure III.4 Latitudinal dependence of the sunset NO_x/NO_y ratio in January 1993 at the levels shown between 68.2 and 4.6 mbar. Model results with and without heterogeneous reactions on sulfate aerosol are shown by red and black lines, respectively. Model results with heterogeneous chemistry and with the reaction rate of $OH + NO_2 + M \rightarrow HNO_3 + M$ reduced by 25% are shown by grey lines. The UARS values are shown by symbols for the two methods of NO_y initialization: blue crosses for NO_y (UARS) and green diamonds for NO_y (CH_4). The UARS values for the N_2O initialization (not shown) are close to those for the NO_y (UARS) approach.

To study model underestimation of the NO_x/NO_y ratio in the stratosphere more carefully, we analyze the sunset vertical profiles of HNO_3, NO, and NO_2 at 45°S (summer) and 35°N (winter) (see Figure III.5). Below 30 mb (about 24 km) and above 6 mb (about 34 km), the model reproduces the observed profiles of these nitrogen species reasonably well. However, the model considerably underestimates NO_2 and overestimates the HNO_3 amount in the 30- to 7-mb range. The reason for this discrepancy is not clear yet, and further analysis is required. Some possible speculations on this issue are discussed in Danilin et al. (1999).

Figure III.6 shows the ground-based concurrent measurements of HNO_3 and NO_2 columns at Lauder (NZ, 45°S, 170°E). Since the measured and modeled values of the HNO_3 columns are in reasonable agreement, the clear model underestimation of the NO_2 column signals about problems with partitioning inside the NO_y family, which could not be explained by the uncertainties of the NO_y initialization.

We saw a similar pattern for the NO_2 ground-based column measurements at the Japanese stations in Moshiri (44°N) and Kiso (36°N). More details of our model analysis are presented in Danilin et al. (1999). A copy of the paper is included as ***Appendix F***.

In addition, we got involved with the Prof. Y. Kondo's group at Nagoya University (Japan) in model analysis of the Improved Limb Atmospheric Spectrometer (ILAS) measurements. Our first joint results are presented in Koike et al. (1999).

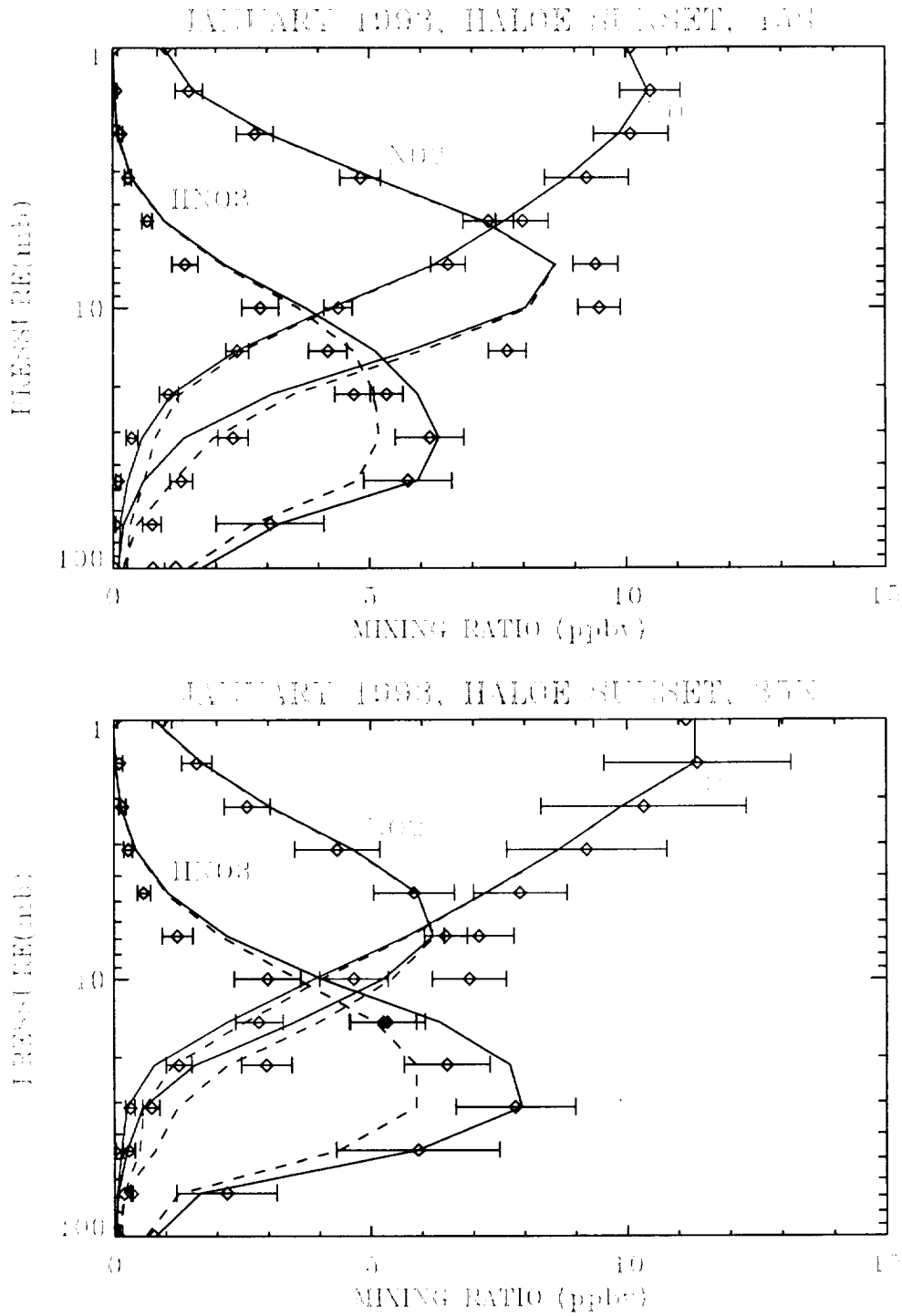

Figure III.5 Vertical profiles of NO (blue), NO_2 (green), and HNO_3 (red) in January 1993 at 45°S (top panel) and 35°N (bottom panel) at sunset. UARS data are shown by symbols with error bars, and model results are shown by solid (with heterogeneous reactions) and dashed (without heterogeneous reactions) lines according to the UARS initialization.

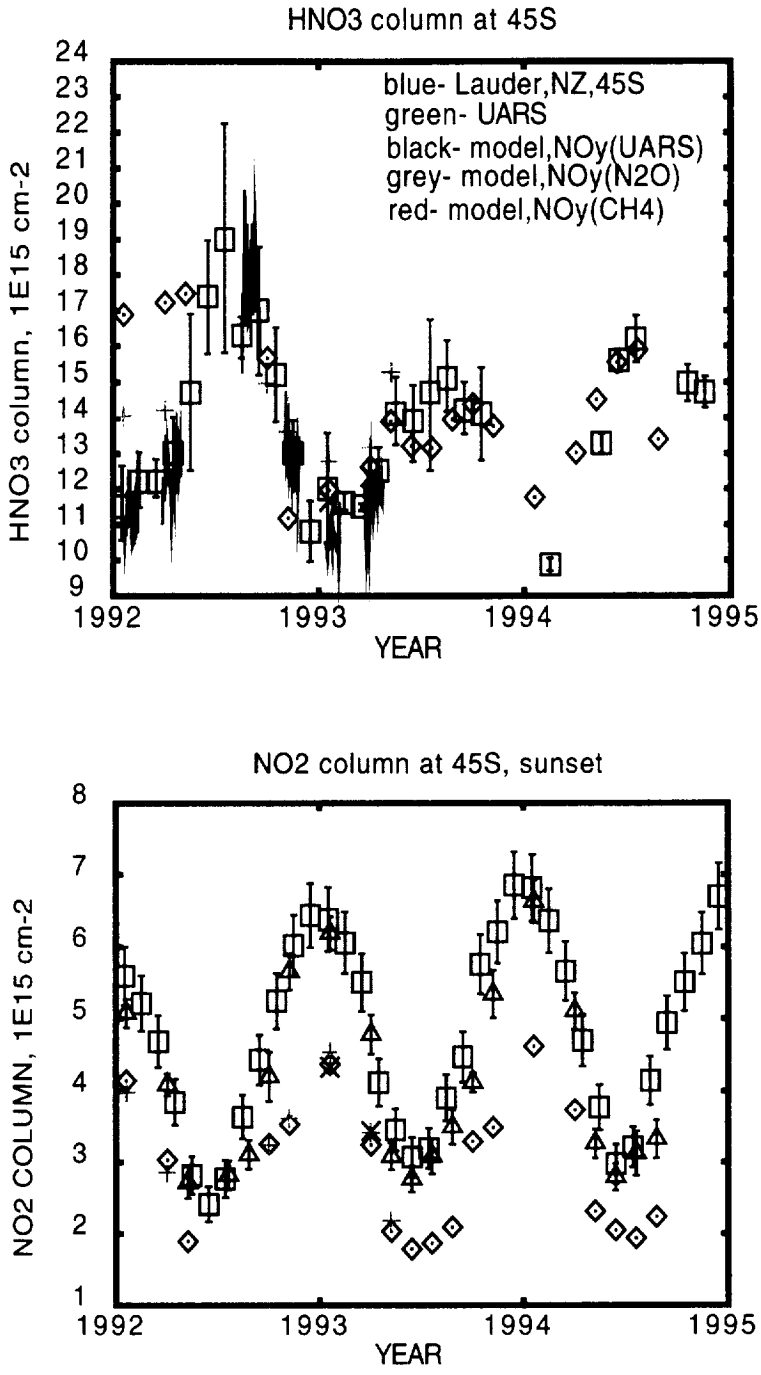

Figure III.6 HNO_3 (top panel) and sunset NO_2 (bottom panel) columns at 45°S between January 1992 and January 1995. Blue squares with error bars show ground-based measurements in Lauder, New Zealand; red diamonds, grey plus signs and black crosses show box model results for the CH_4, N_2O, and UARS initializations, respectively. Green curves in the top panel depict daily HNO_3 column values at 44°S according to the CLAES instrument (version 8). Green triangles with error bars in the bottom panel show monthly and zonally averaged HALOE (version 18) values of the sunset NO_2 column. The box model and UARS data are increased by partial HNO_3 and NO_2 columns below 100 mbar (see text).

III.3 Evaluation of New Rates for NO_y Partitioning Reactions

Recent airborne measurements of NO and NO_y obtained during the POLARIS campaign, mostly at high northern latitudes in summer, indicate that the NO_x/NO_y partitioning calculated by models for the lower stratosphere is systematically underpredicted. Recent measurements of reaction rate constants which control NO_x/NO_y partitioning offer a possible resolution to the model/measurement disagreement. In collaboration with David Fahey's group at NOAA in Boulder who made the NO and NO_y measurements during the POLARIS campaign, we have performed model sensitivity studies to evaluate the effects of these rate revisions.

In the summer months at high latitudes, heterogeneous reactions do not play a large role in controlling the NO_x/NO_y ratio. Under these conditions, the ratio is largely controlled by the following reactions:

$$OH + NO \rightarrow HNO3 + M \quad (R1)$$
$$OH + HNO_3 \rightarrow NO_3 + H_2O \quad (R2)$$
$$HNO_3 + hv \rightarrow OH + NO_2 \quad (R2)$$

The rates for reactions R1 and R2 reported in JPL-97 (DeMore et al., 1997) have recently been questioned. Donahue et al. (1997) first suggested that the rate for reaction R1 reported in JPL-97 may be too high. Dransfield et al. (1998) and Brown et al. (1999a) reported new values for the rate of reaction R1 for stratospheric conditions which are about 20% lower than JPL-97 values. Brown et al. (1999a) also reported values of the rate constant for R2 which are higher than the JPL-97 recommendation. Using a photochemical steady state box model, Gao et al. (1999) determined that agreement between models and measurements of NO_x/NO_y is much improved with the Brown et al. (1999a) rates for R1 and R2 relative to the JPL-97 rates (model/measurement ratio increases from 0.62 to 0.84).

The Brown et al. (1999a) rates for R1 and R2 have been incorporated into the AER 2-D chemical transport model. Figure III.7a shows the change in calculated ozone for June of 2015 with subsonic aircraft included due to the modified rates relative to the JPL-97 rates. Ozone reductions of up to 5% are seen between 20 and 40 km altitude, while ozone increases are seen in the troposphere. Changes in ozone column (Figure III.7b) exceed 1% only in northern polar regions. The percentage of ozone loss due to NO_x increases by 2-8% in the lower stratosphere, while that due to HO_x and ClO_x decreases. This change in the relative importance of the ozone loss cycles modifies the sensitivity of ozone to perturbations.

A new rate constant has also been measured for the reaction of NO_2 with O:

$$NO_2 + O \rightarrow NO + O_2 \quad . \quad (R4)$$

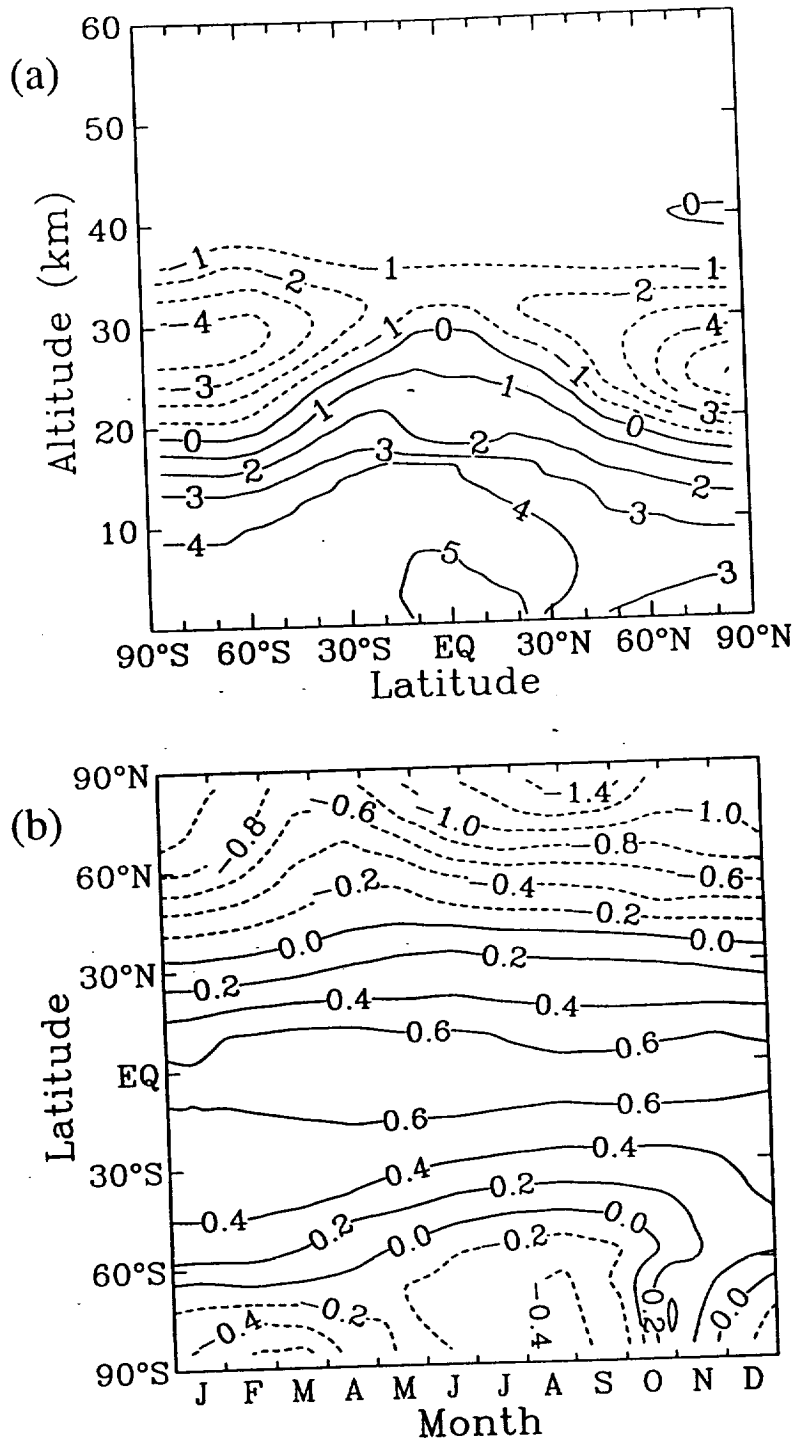

Figure III.7 Calculated percentage change in (a) local ozone in June, and (b) total column ozone due to modifying the rates for reactions R1 and R2 from JPL-97 values to those reported by Brown et al. (1998). Results shown are for 2015 with subsonic aircraft emission included.

This reaction does not affect the NO_x/NO_y partitioning significantly, but is a loss mechanism for odd oxygen. The new rate (A.R. Ravishankara, personal communication, 1998) is about 30% higher than the JPL-97 value at 200 K. Figure III.8 shows the calculated changes in ozone due to inclusion of this modified reaction, along with R1 and R2, in the AER 2-D model. Local ozone is reduced by up to 13% at 30 km in the high latitude, up to 6% at the equator at 30 km, and increased in the troposphere. Column ozone is reduced by 1-7% relative to a model with the JPL-97 rates.

We have calculated the ozone change due to HSCT emissions in 2015 (with 3.0 ppbv of Cl_y) and 2050 (with 2.0 ppbv of Cl_y) under two different emission scenarios. Both scenarios include 500 HSCTs operating at Mach 2.4 at 18-20 km altitude with an emission index (E1) for NO_x of 5, but scenario 1 includes no sulfur emissions, while scenario 2 includes sulfur emissions assuming $EI(SO_2)$=0.4 and 50% conversion of the emitted sulfur to small particles in the aircraft wake. Table III.1 summarizes the calculated annual average ozone column changes at 60°N. Without sulfur emissions, the Brown et al. rates for R1 and R2 lead to a slight increase in ozone depletion due to HSCT because of the increased importance of the NO_x cycle for ozone loss. With sulfur emissions, the new rates have the opposite effect. Ozone depletion due to emitted sulfur (which increases the stratospheric aerosol burden) is a function of the HO_x and ClO_x cycles, which are reduced under the new chemistry. Including new rates for reactions R1, R2 and R4 leads to even more ozone depletion due to HSCT for scenario 1 and even less ozone depletion for scenario 2. With R1, R2 and R4 updated, column ozone depletion at 60°N in 2015 is the same with or without sulfur emissions, and in 2050, column ozone depletion is greater without sulfur emissions than with sulfur emissions.

Table III.1 Annual average column ozone change at 60°N due to a fleet of 500 HSCTs operating at Mach 2.4 with $EI(NO_x)$=5 in the year 2015 or 2050

HSCT	$EI(SO_2)$	with JPL-97 rates		R1, R2 updated		R1, R2, R4 updated	
Scenario		2015	2050	2015	2050	2015	2050
1	0	-0.5%	-0.5%	-0.6%	-0.6%	-0.8	-0.7
2	0.4	-1.3%	-0.9%	-1.0%	-0.5%	-0.8	-0.4

The result of this study is published in GRL (Gao et al., 1999). A copy of the paper is included as ***Appendix G.***

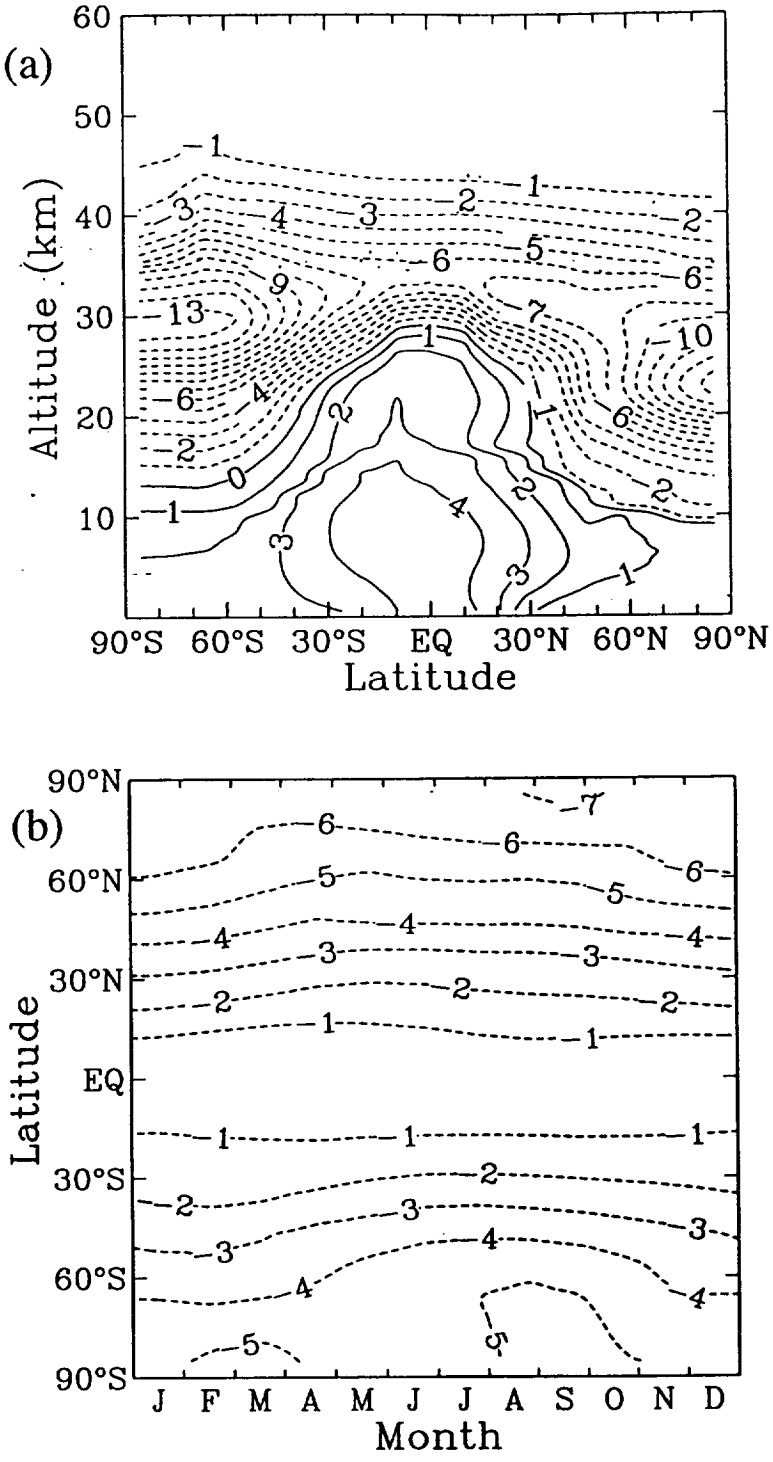

Figure III.8 Calculated percentage change in (a) local ozone in June, and (b) total column ozone due to modifying the rates for reactions R1, R2, and R4 from JPL-97 values to those reported by Brown et al. (1998) and Ravishankara (personal communication, 1998). Results shown are for 2015 with subsonic aircraft emission included.

IV. Ozone Assessment Studies

IV.1 ODP of CH_3Br

The AER 2-D CTM was used to compute the Ozone Depletion Potential (ODP) and the Bromine Efficiency Factor (BEF) of CH_3Br. Several key rate constants were revised in JPL-97 (DeMore et al., 1997) with new values significantly different from previous JPL-94 (DeMore et al., 1994) values. These include:

$$BrO + HO_2 \rightarrow HOBr + O_2 \quad (1)$$

$$BrNO_3 + H_2O \text{ (aerosol)} \rightarrow HOBr + HNO_3 \quad (2)$$

$$BrNO_3 + hv \rightarrow BrO + NO_2 \quad (3a)$$

$$\rightarrow Br + NO_3 \quad (3b)$$

Li et al. (Stanley Sanders, private communication) reported a rate constant for reaction (1), the rate limiting step of the BrO_x/HO_x cycle, which is effectively a factor of two smaller at stratospheric temperatures than the previous JPL-94 rate. A new expression for the sticking coefficient for heterogeneous reaction (2) was given by Hanson et al. (1996). The sticking coefficient of reaction (2) is now dependent on temperature and water vapor, with a maximum value of 0.8 in cold polar regions, replacing a constant sticking coefficient of 0.4 (Hanson and Ravishankara, 1995). Photolysis cross sections for reaction (3), recommended by JPL-94, are based on measurements by Spencer and Rowland (1978) and assume a 100% yield via channel (3b). Nickolaisen and Sander (Stanley Sanders, private communication) indicate a probable product branching for reaction (3) with 74% proceeding along branch (3a) and 26% along (3b). Note that in contrast to (3b), reaction (3a) does not lead to ozone loss (i.e. a null cycle). We used the AER 2-D chemistry transport model (CTM) to assess the implications of the above reaction rate changes on the ODP and BEF of CH_3Br. By combining the calculated ODP/BLP ratio with the latest estimate of 0.7 year for the atmospheric lifetime of CH_3Br, the likely value of ODP for CH_3Br is 0.39. The model calculated concentration of HBr (~ 0.3 pptv) in the lower stratosphere is substantially smaller than the reported measured value of about 1.5 pptv. The model can reproduce the measured value of 1.5 pptv if one assumes a yield for HBr of 1.3% from the reaction of BrO+OH, or a yield of 0.6% from the reaction of $BrO + HO_2$. Our calculations show that the effect of these assumed rates on the model calculated ODP/BLP ratio is minimal: practically no impact for the assumed BrO+OH yield and 10% smaller for the $BrO+HO_2$ case.

The results were published in Journal of Geophysical Research (Ko et al., 1998). A reprint of the paper is included as ***Appendix H***.

IV.2 National Research Council Committee on Assessment of Fire Suppression Substitutes and Alternatives to Halon

Malcolm Ko was invited to participate in preparation of a report by the National Research Council. The title of the Report is *Fire Suppression Substitutes and Alternatives to Halon for the U.S. Navy Application*. Malcolm Ko was a member on the Committee on Assessment of Fire Suppression Substitutes and Alternatives to Halon, which is responsible for the study performed for the Naval Studies Board of the National Research Council.

Halons are highly effective as fire fighting agents and are widely used on board Navy ships and aircrafts. With the Montreal Protocol agreement, halons are no longer manufactured in the U.S. The Navy is given an exemption on mission-critical uses until the current halon supply is exhausted. The Committee was convened to assess the science and engineering information relevant to identification and evaluation of alternative agents that could be developed to replace halons. The scope includes possibilities of drop-in replacements as well as alternative systems.

Malcolm Ko worked with several atmospheric scientists in the Committee to prepare a chapter summarizing the current knowledge on the atmospheric chemistry and evaluation of environmental effects of fire suppressants. A copy of the chapter is included in ***Appendix I***.

IV.3 Contributions to the 1998 *WMO Ozone Assessment Report*

Malcolm Ko was a co-author for Chapter 1, "Long-lived Ozone-Related Compounds", of the *WMO Ozone Assessment Report*. The lead authors were Ronald Prinn and Rudolf Zander. Malcolm Ko worked with Michael Volk to prepare a section on the atmospheric lifetimes of the long-lived gases as can be determined from model calculations and observations. Malcolm Ko attended the Chapter co-authors meeting in January 1998 at Boulder Colorado, and worked with the lead authors to revise the chapter after the Review meeting in June, 1998.

Jose Rodriguez was lead author for Chapter 2 along with Michael Kurylo. Jose's effort was funded by this project. Chapter 2, entitled "Short-lived Ozone-related Compounds", deals with source gases that are removed by OH in the troposphere. A large part of the chapter was devoted to methyl bromine (CH_3Br), including its ozone depletion potential. Jose attended the co-authors meeting for Chapter 2 in January 1998 at Boulder Colorado. He also attended the Review meeting held in Les Diablet, Switzerland in June, 1998.

Debra Weisenstein was a contributor for Chapter 12, "Predicting Future Ozone Changes and Detection of Recovery". Results from the AER 2-D model for Scenario A (1970-1995) and Scenario A3 (1996-2050) are shown in the report for comparison of model results with past trends and for predictions of future ozone change. In addition, AER contributed a modeling study for the 1979-1995 period in which the effects of using year-by-year temperature variability

was contrasted with use of climatological temperatures. The periods 1984-86, 1988-91, and 1992-95 show less ozone depletion with year-by-year temperatures than with climatological temperatures.

IV.3a Summary of Analyses Performed in Preparation of Chapter 1

The previous WMO sssessment report (WMO, 1995) gave a set of reference steady-state lifetimes for use in calculations of ozone depletion potentials and global warming potentials. The same reference lifetimes were also used as response times in halogen loading calculations. With the exception of CFC-11, the WMO (1995) reference lifetimes for the species listed are the mean values of model results from several groups reported in Kaye et al. (1994). Because CFC-11 is used as the reference gas in the definition of the ozone depletion potential, extra care was used in selecting its WMO (1995) reference value, basing it on observations as well as model calculations.

The model calculated lifetimes for the current WMO assessment report (WMO, 1998) are taken from the Models and Measurements Workshop II calculations. Table IV.1 lists the model calculated steady state lifetimes. Several 2-D models modified their transport parameters to simulate the effect of a tropical barrier. Results from the AER model show that restricting the mixing through the barrier leads to shorter calculated lifetimes (Shia et al., 1998). A second observation is that the lifetimes for CFC-11 and CCl_4 from two of the three 3-D models are much shorter than those calculated by the 2-D models. It could be argued that lifetimes calculated by 3-D models may be more realistic since they have a more direct (i.e., 3-D) representation of the transport processes in the atmosphere. However, more work is needed to assure that the vertical resolution in such models is sufficient to resolve the scale heights of the species with short local lifetimes.

The observational results are taken from Volk et al. (1997) which uses historical records of tropospheric measurements to correct the observed correlation in the lower stratosphere to obtain steady state lifetimes. The Volk et al. (1997) formalism provides, for the first time, a way to obtain steady-state stratospheric lifetimes from observations. With the exception of Halon-1211, the species listed in Table IV.2 have very little removal in the troposphere. As a result, the derived stratospheric lifetimes can be compared directly to atmospheric lifetimes. As is evident in Table IV.2, the derived lifetimes for CFC-11, CCl_4, and CFC-12 are in the shorter end of the model range, and shorter than the WMO (1995) reference lifetimes (see Table IV.3). It is also interesting to note that the derived shorter lifetimes are in better agreement with the lifetimes calculated by two of the three 3-D models in Table VI.1. The large uncertainties in the derived lifetimes given in column 3 of Table IV.2 arise from the uncertainty in the SF_6 measurement

Table IV.1 Model-calculated Steady-state Lifetimes in Years

SPECIES	AER[a]	GSFC[a]	CSIRO[a]	Harvard 2-D[a]	LLNL[a]	SUNY -SPB[a]	UNIVAQ 2-D[a]	LaRC 3-D[a]	GISS-UCI 3-D[b]	MIT 3-D[c]
N_2O	109	130	117	122	106	125	122	175	113	124
CCl_3F	47	61	53	68	49	49	44	57	35	42
CCl_2F_2	92	111	100	106	92	107	105	149	90	107
$C_2Cl_3F_3$	77	101	83	55	81	87	81	-	70	79
CCl_4	41	53	46	64	42	39	36	42	28	30
$CBrClF_2$ (H-1211)	16[d]	12[e]	36[f]	-	-	-	21[f]	29[f]	21	-
$CBrF_3$ (H-1301)	63	78	69	-	-	-	61	93	52	-

[a] Results are taken from the Model and Measurement Workshop II (M&M II). The models and the contact persons are as follows: AER - Atmospheric and Environmental Research, Inc., USA, Malcolm Ko; GSFC - NASA Goddard Space Flight Center, USA, Charles Jackman; CSIRO - Commonwealth Scientific and Industrial Research Organisation (CSIRO) Telecommunications and Industrial Physics, Australia, Keith Ryan; Harvard 2-D - Harvard University, Hans Schneider; LLNL - Lawrence Livermore National Laboratory, USA, Doug Kinnison; SUNY-SPB - State University of New York at Stony Brook, Marvin Geller; UNIVAQ 2-D - University of l'Aquila, Italy, Giovanni Pitari; LaRC 3-D - NASA Langley Research Center, USA, William Grose. LaRC is the only 3-D model that participated in M&M II.

[b] Results given are for steady-state lifetimes from Avallone and Prather (1997). The values should be close to the atmospheric lifetimes except for Halon-1211.

[c] Results for MIT model from Table 5-2 of Kaye *et al.* (1994). MIT model described in Golombek and Prinn (1993) and references therein.

[d] Calculated using cross section from Burkholder *et al.* (1991).

[e] Calculated using cross section from DeMore *et al.* (1997).

[f] Calculated using the Halon-1211 cross section from DeMore *et al.* (1997) that did not give any recommendation beyond 288 nm.

Table IV.2 Stratospheric Steady-state Lifetimes (from *Volk et al.*, 1997)

Species	Observed $d\chi_i/d\Gamma$ from ASHOE/MAESA (ppt yr^{-1}, ±%)	Steady-state lifetime based on corrected gradient with respect to age (years ± years)	$d\chi_i/d\chi_{CFC\text{-}11}$ observed correlation slope relative to CFC-11 from ASHOE/MAESA (ppt/ppt, ± %)	Steady-state lifetime based on corrected correlation slope and $\tau_{CFC\text{-}11}$ = 45 ± 7 years (years ± years)	Correction factor for tropospheric growth $C(\chi_i)$
N_2O	-13,000 ± 38%	124 ± 49	436 ± 11%	122 ± 22	0.97 ± 0.02
CCl_3F	-33.5 ± 28%	41 ± 12		(45 ± 7)	0.96 ± 0.02
CCl_2F_2	-43.8 ± 25%	77 ± 26	1.29 ± 7%	87 ± 17	0.77 ± 0.07
CCl_2FCClF_2	-7.3 ± 22%	89 ± 35	0.212 ± 20%	100 ± 32	0.65 ± 0.12
CCl_4	-15.9 ± 32%	32 ± 11	0.515 ± 3.6%	32 ± 6	1.03 ± 0.02
$CBrClF_2$ (H-1211)	-0.84 ± 31%	20 ± 9	0.0237 ± 7%	24 ± 6	0.90 ± 0.10

made during the 1994 ASHOE/MAESA campaign. The uncertainty has been reduced in subsequent flights. The lifetimes relative to CFC-11 derived by Volk et al. (1997) have much smaller uncertainties because $d\chi_i / d\chi_{CFC\text{-}11}$ can be determined more accurately. When referenced to a CFC-11 lifetime of either 45 years (Table IV.3, column 6) or 50 years (Table IV.3, column 5), with the exception of CCl_4 and Halon-1211, these derived lifetimes agree within their uncertainties and with the WMO (1995) reference lifetimes.

Butler et al. (1998) showed that the observed burden of Halon-1211 is inconsistent with the emissions if one uses the reference lifetime of 20 years. The WMO (1995) reference lifetime of 20 years was obtained by averaging the model results from Kaye et al. (1994). Because of disagreement between the measurements of Gillotay and Simon (1989) and Burkholder et al. (1991) for the absorption cross sections for wavelengths longer than 288 nm, the JPL Data Evaluation Panel did not give any recommended values for these wavelengths (DeMore et al., 1997). Burkholder et al. (1991) estimated the partial lifetime due to photolysis in the long-wavelength region to be about 20 years. Combining this with the estimated stratospheric lifetime of 20 years from Volk et al. (1997) would give an atmospheric lifetime of about 10 years. Table IV.1 shows calculated lifetimes from several models with different cross-sections. It is likely that some models ignored the long wave photolysis in their calculations and biased the average towards longer lifetimes.

The WMO (1995) value of 50 years for CFC-11 is in good agreement with the central estimate of the lifetime from ALE/GAGE/AGAGE measurements (Cunnold et al., 1997), but not with the central estimate of 41 years by Volk et al. (1997). The derived lifetime range for CFC-11 using the Volk et al. (1997) method (29 to 53 years) just includes the value of 50 years. However, a new reference value between 41 and 50 years would lie well within the ranges of both the Cunnold et al. (1997) and Volk et al. (1997) estimates.

One result of the study is that there are indications that the lifetime of CFC-11 may be shorter than the currently accepted value of 50 years. A clearer picture should emerge when the uncertainty in the lifetime can be reduced. One conclusion of the Chapter is that the reference lifetime of CFC-11 and some of the other gases should be re-evaluated given the new information available since the Kaye et al. (1994) lifetime report.

Table IV.3 Comparison of Reference Steady-state Lifetimes from *WMO* (1995) with Model-calculated Ranges and Lifetimes Derived from Observations. All Lifetimes are in Years.

	Reference Lifetimes from WMO [1995] [a]	Model Range [b]	Volk SF_6 [c]	Volk CFC-11 [d] (50 Year)	Volk CFC-11 [d] (45 Year)	Minschwaner UARS [g]	AGAGE [e]
N_2O	120	106-175	124 ± 49	135 ± 16	122 ± 22	117 ± 26	
CCl_3F	50	35-68	41 ± 12	50[d]	(45 ± 7)		52 (40-76)
CCl_2F_2	102	90-149	77 ± 26	96 ± 12	87 ± 17	103 ± 25	185 (105-770)
$C_2Cl_3F_3$	85	55-101	89 ± 35	112 ± 31	100 ± 32		
CCl_4	42	28-64	32 ± 11	36 ± 4	32 ± 6		
$CBrClF_2$ (H-1211)	20	12-36	20 ± 9[f]	26 ± 5[f]	24 ± 6		
$CBrF_3$ (H-1301)	65	61-93					

[a] From Table 13-1, WMO (1995).
[b] From Table 1-4.
[c] Derived steady-state stratospheric lifetimes based on gradient with age derived from SF_6 data, from Volk *et al.* (1997).
[d] Derived steady-state stratospheric lifetimes based on gradient with CFC-11 and an adopted lifetime of 50 years for CFC-11, from WMO (1995). Compare to values based on 45 years from Table 1-5.
[e] From Table 1-6. The range is calculated using the uncertainty in the inverse lifetime given in the table.
[f] Since Halon-1211 is dissociated by photolysis in the longwave, there is significant removal in the troposphere so that the stratospheric lifetimes should not be compared directly to the global lifetime. See text for further discussion.
[g] Steady-state lifetime from Minschwaner *et al.* (1998) derived using UARS observations, assumed mean age, and tropospheric growth rates.

IV.3b Model Simulation of the Future Behavior of Ozone Through 2050

AER provided 2-D model calculations of past and future ozone trends for Chapter 12 of the WMO/UNEP 1998 Ozone Assessment. Chapter 12 is entitled "Predicting Future Ozone Changes and Detection of Recovery" with lead authors John Pyle and David Hofmann. Section 12.2 deals with calculationed ozone changes and was authored by Doug Kinnison. AER provided calculated results for Scenario A from 1979 to 1995 and Scenario A3 from 1996 to 2050. Figure 12.9 of the report shows these results and is reproduced here as Figure IV.1. These calculations used year-by-year temperatures from NCEP. A plot of the AER calculated ozone trends from 1979 to 1995 using both climatological and year-by-year temperatures appears as Figure 12.7 in the report and as Figure IV.2 here.

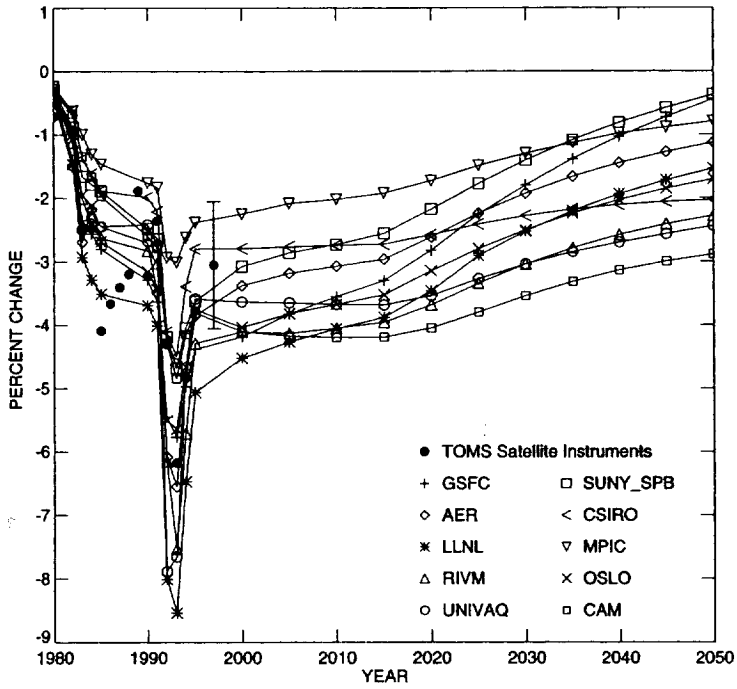

Figure IV.1 Time variation in Cl_y (top panel) and Br_y (bottom panel) mixing ratios at 20 km, 50°N latitude, as determined from 10 models.

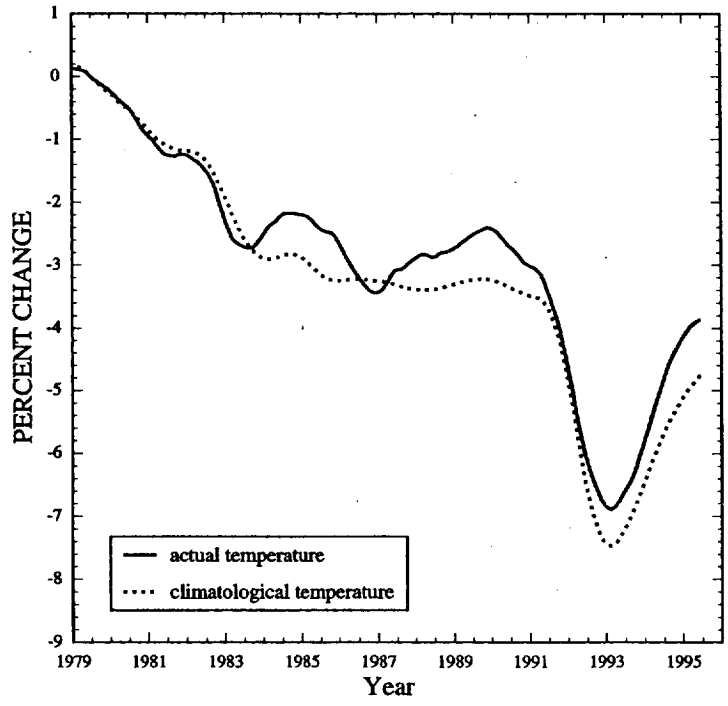

Figure IV.2 Percentage change in global (65°S-65°N) column ozone using a 24-month running mean for the AER model. The solid line represents an integration that includes the use of the mean temperature and temperature probability distribution about the zonal mean taken for each year between 1979 and 1995. The dashed line uses an 8-year average of both mean temperature and temperature probability distributions.

At the Spring 1998 AGU meeting in Boston, Debra Weisenstein presented a poster entitled "Calculations of ozone trends in the AER 2-D model: Sensitivity to interannual temperature variations and transport barriers." The study presented included the ozone trend calculations from 1979 to 1995 generated for WMO and additional sensitivity studies for the same time period. To study sensitivity to input temperature and aerosol surface area, the calculation was performed with (A) only trace gas increases; (B) with trace gas increases and aerosol surface area variations; (C) with trace gas increases, aerosol surface area variations, and zonal mean temperature variations; and (D) with trace gas incerases, aerosol surface area variations, and variations in both the zonal mean and distribution of temperature. Figure IV.3 shows the calculated change in annual average column ozone from 1979-1995 for the 4 scenarios just mentioned. It can be seen that use of year-by-year temperatures in the model add variability to the calculated ozone trends, though disagreements with TOMS data remain. The lack of year-by-year variations in transport is one possible explanation.

Transport sensitivities were approached by repeating the 1979-1995 trend calculations with two alternate circulations. The first, designated the "AER Slow Circulation", was derived by scaling the advective winds in the standard AER model by 0.6 to slow down the transport. The second transport circulation employed both the advective winds and eddy diffusion coefficients of the GSFC 2-D model. Both these alternate circulations produce total ozone maps for 1990 which resemble the TOMS data more closely than the standard AER model. Calculated ozone trends with these circulations are shown in Figure IV.4. The two AER circulations produce very similar ozone trends. The GSFC circulation yields excessive ozone depletion in 1993, a results of excessive depletion in the southern hemisphere for that year.

A copy of the presentation made at the AGU meeting is included as ***Appendix C.***

IV.4 Contributions to the IPCC Special Report on Aviation and the Global Atmosphere

The International Panel on Climate Change (IPCC), at the request of the International Civil Aviation Organization (ICAO) and the Parties to the Montreal Protocol on Substances that Deplete the Ozone Layer, decided in 1996 to produce a Special Report on *Aviation and the Global* Atmosphere (IPCC, 1999), with the purpose of assessing the consequences of greenhouse gas emissions from aircraft engines. The report considers all the gases and particles emitted by aircraft into the upper atmosphere and the role that they play in modifying the chemical properties of the atmosphere and initiating the formation of contrails and cirrus clouds. The radiative effects of these changes are considered along with changes in ozone and subsequent modifications to uv radiation reaching the surface. Modeling work in support of the IPCC

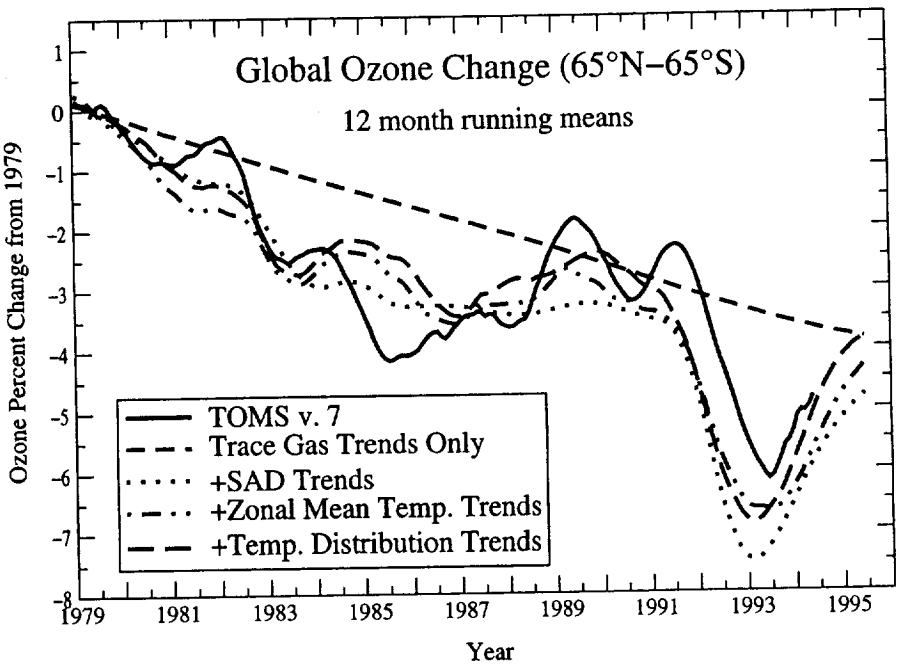

Figure IV.3 Percent change in global (65°S-65°N) ozone column relative to 1979 as calculated by the AER model from 1979 to 1995 and as observed by TOMS instrument. Four versions of model results include: (1) trends in trace gases only, (2) trends in trace gases and aerosol, surface and density, (3) also include trends in zonal mean temperatures from NCEP, and (4) additionally include changes in temperature distribution from NCEP.

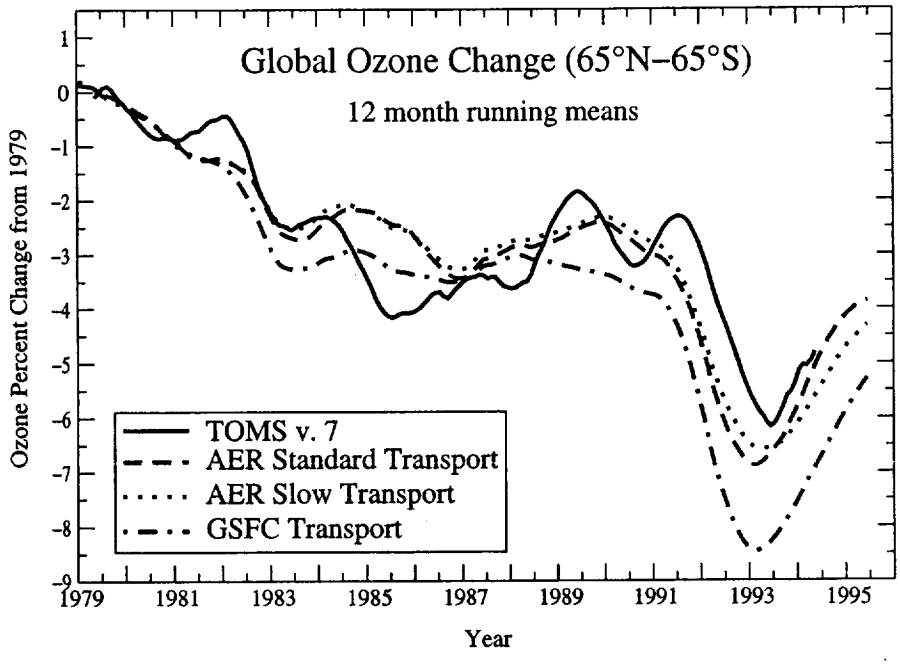

Figure IV.4 Percent change in global (65°S-65°N) ozone column relative to 1979 as calculated by the AER model and observed by TOMS instrument. Three versions of model results use different transport circulations: (1) the standard AER transport, (2) the slow AER transport (streamfunction multiplied by 0.6), and (3) the GSFC 2-D Model Transport.

Special Report was performed by AER in 1997 and 1998. This participation was made possible by the long history of model development work funded by ACMAP.

Chapter 4 of the IPCC Special Report dealt with model-calculated impacts of aircraft emissions from subsonic and supersonic aircraft on atmospheric NO_x, H_2O, O_3 and aerosol abundance. AER was involved mainly in the supersonic emission calculations. The description of models used in the supersonic assessment (Section 4.3.1 of the Special Report) was written by Malcolm Ko. Aircraft emission scenarios were given for fleets of either 500 or 1000 HSCTs and parametrically varied the emission index (EI) of NOx, the sulfur emission, the flight altitude, and background atmospheric conditions. The AER 2-D sulfate aerosol model provided calculations of change in stratospheric aerosol surface area density (SAD) due to aircraft emission of sulfur which were used as scenario input by all modelers. Due to uncertainties in the extent of gas-to-particle conversion in the plume, this parameter was varied parametrically also, with values of 0%, 10%, 50%, or 100% employed. There were nine different SAD perturbation fields calculated, including variations in cruise altitude and fleet size, but assuming EI(S) of 0.2 for all. A total of 35 HSCT scenarios were analyzed for 2015 and 14 scenarios for 2050.

Scenario calculations were run by six 2-D models and three 3-D models, though not all models performed calculations for every scenario. Calculated perturbations in NO_y and H_2O maximized in the northern hemisphere lower stratosphere, with maximum perturbations to NO_y ranging from 0.6 to 1.0 ppbv and perturbation to H_2O ranging from 0.4 to 0.7 ppmv under Scenario S1c with used the most probable EI(NO_x) of 5 gm (NO_2)/(kg fuel) and EI(H_2O) of 1230 gm/(kg fuel) along with the standard cruise altitude of about 19 km. It is found that emission of H_2O dominates the ozone response under these conditions, which ranges from -0.4% to 0% for the northern hemisphere column perturbation. The sensitivity of ozone response to EI(NO_x) varied widely among the models, with both positive and negative sensitivities found under nonvolcanic background aerosol conditions (SA0). However, under enhanced background aerosol conditions (4xSA0), all models calculate a positive ozone response to increasing EI(NO_x). Aircraft sulfur emissions have a significant impact on stratospheric ozone. With 10% of the sulfur assumed to be converted to particles in the plume (Scenario S1k), northern hemisphere average ozone column changes range from -0.8% to -0.2%. With 50% of the sulfur assumed to be converted to particles in the plume (Scenario S1f), northern hemisphere average ozone column changes range from -1.1% to -0.4%. See the full Special Report for more details.

The IPCC Technical Report, entitled *Model Calculations of the Atmospheric Effects of Supersonic Aviations Which Were Used in the IPCC Special Report on Aviation and the Global Atmosphere,* was compiled to provide additional detail regarding the supersonic emission scenario calculations presented in IPCC Chapter 4. Due to the space limitations in the Special Report, detailed plots and discussion for a majority of the model calculations were omitted. The

technical report was intended to fill that gap and was compiled for two reasons: (1) to aid those called upon to review the IPCC Special Report, and (2) to archive and document the calculations performed by nine modeling groups for up to 50 scenarios each. It does not attempt to provide a synthesis of the modeling results or draw conclusions regarding the impact of aircraft on the atmosphere.

The 500 page IPCC Technical Report consists of 5 chapters covering (1) detailed model descriptions, (2) emission scenarios, (3) the background atmosphere as calculated for 2015 and 2050, (4) HSCT perturbations calculated for 2015, and (5) HSCT perturbations calculated for 2050. It has been published in electronic form only and may be obtained via ftp download in postscript (.ps) or Adobe Acrobat (.pdf) formats at the following locations:

ftp://typhoon.larc.nasa.gov/pub/Sage/IPCC_TECH_REPORTS/supersonic/report
ftp://ftp.aer.com/IPCC_TECH_REPORT (not for web browsers)
ftp://anonymous@ftp.aer.com/IPCC_TECH_REPORT (for web browsers)

and additionally can be read online via a web browser at:

http://asd-www.larc.nasa.gov/sage/IPCC_TECH_REPORTS/tech.html
http://www.aer.com/groups/chem/ipcc_report/.

IV.5 Participation in EPA Workshop on Ozone Depletion Potential of Short-lived Source Gases

Emissions of halogenated gases containing chlorine, bromine or iodine have the potential to affect stratospheric ozone concentrations if sufficient amounts of these compounds or their degradation products reach the stratosphere. As a result of the Montreal protocol and the Clean Air Act, the U.S. Environmental Protection Agency regulates the use of such chemicals through consideration of the Ozone Depletion Potential (ODP) for each compound. Traditionally, ODPs have been primarily evaluated through the use of zonally-averaged, two-dimensional chemical-transport models of the global atmosphere. These models have been the primary tools used in studies of stratospheric processes. As most chemicals evaluated for ODP in the past have atmospheric lifetimes that are sufficiently long that they would be well mixed in the troposphere, the two-dimensional model has been an adequate tool for studies of ODP. However, a number of the compounds recently being proposed as replacements for substances controlled under the Montreal Protocol have extremely short atmospheric lifetimes, on the order of days to a few months. An important example is n-propyl bromide (also referred to as 1-bromo-propane, $CH_2BrCH_2CH_3$ or simplified as C_3H_7Br or nPB), which has an atmospheric lifetime of about 11

days and is being considered as a solvent. Because nPB contains bromine, any amount reaching the stratosphere has the potential to affect concentrations of stratospheric ozone.

After emission, such short-lived chemicals would not be expected to have well mixed concentrations in the troposphere. Following emission into the atmosphere, generally at midlatitudes in the northern hemisphere, winds and other mixing processes in the atmosphere would gradually transport these gases to the tropics where they can most effectively be transported to the lower stratosphere. At the same time, because of their short lifetimes, reaction with OH and other chemical loss processes would convert a significant fraction of the chemical emitted to its degradation products. One must also consider the processes affecting the resulting degradation products as they could act as vehicles for transporting chlorine or bromine to the lower stratosphere. The question of how much of the halogen would be available to affect stratospheric ozone therefore depends greatly on the complex effects of transport and chemical processes in the troposphere. The two-dimensional models, because of their zonally-averaged nature, are not designed to adequately account for the variations in concentration and transport of such short lived compounds and their degradation products. As a result, there are questions about the adequacy of the ODPs determined with these models for such chemicals. Malcolm Ko and Don Wuebbles (University of Illinois) assisted EPA and NASA to convene a special workshop on March 30-31, 1999 to discuss some of these issues. This Workshop brought together key members of the international scientific community to discuss how more meaningful analyses of the effects of short-lived compounds (lifetimes on the order of days to a few months) on stratospheric ozone can be made. The purpose was to provide a list of priorities for scientific studies over the next nine to fifteen months so that effective policy for the protection of stratospheric ozone can be made relative to the Montreal Protocol for such chemicals. Basically, how can we more effectively determine how much of the bromine or chlorine or iodine from these compounds actually reaches the stratosphere, and then is available to affect ozone? The focus of the discussion was on the following issues:

1. No single number representing an ODP for short-lived ozone depleting substances (ODSs) is scientifically supportable. EPA will need to revisit their policy process (currently based on single-valued ODP's) in light of this fact. New measures, such as quantitatively defined regulations (rather than allow/disallow) will probably be needed.
2. ODPs for short-lived ODSs will need to be defined as a function of location and time of emission. Since emissions from uses of such gases are generally thought to be relatively constant throughout the year, it was suggested that the ODPs could primarily be defined in terms of location of emission.

3. Current 3-D models can provide a matrix of measures (equivalent chlorine loading being preferred) which represent the impacts of a given quantity of a particular substance emitted at different places in different seasons. Each compound requires a separate matrix. The matrices are linked to the currently used ODP (or single value of equivalent chlorine loading) for long-lived ODSs in that, as the atmospheric lifetime of the substance under consideration increases, all of the matrix entries for the substance converge to a single value. The matrix entries for short-lived ODSs are likely to be more reliable in a relative sense than in absolute terms.
4. 3-D models must be evaluated by comparison with real atmospheric measurements. This will likely take several years.
5. In the near term, in order to get an improved evaluation of ODPs for short-lived chemicals like nPB over the next nine to fifteen months, we need to look at realistically achievable goals for determining the ODP matrix as a function of location using existing models. The results from three-dimensional model studies can be used to modify two-dimensional model results to provide an estimate of the ODP matrix for such chemicals. The role of reaction by-products needs to be carefully considered in such studies.
6. Models of stratospheric processes need to consider updates to (a) account for short-lived natural sources of bromine and chlorine and (b) better account for the age of air.

V. Model and Measurement Workshop

The Models and Measurements II Workshop (MMII) was held in the fall of 1997 and the report (Park et al., 1999) finalized in the fall of 1998. This was a follow-on from the initial Models and Measurements Workshop (Prather and Remsberg, 1993) held in 1992. The goal of the workshop was to establish the credibility of two- and three-dimensional assessment models by comparisons with observational data. UARS satellite data were primarily used in the middle and upper stratosphere, while *in situ* data from the numerous aircraft campaigns between 1992 and 1998 were used for the lower stratospheric validation. In addition to the satellite and *in situ* measurements, an ozone climatology was compiled for the validation effort. This climatology was comprised of both satellite (SAGE II, TOMS) and ozone sonde measurements. While the first Models and Measurements Workshop emphasized the chemical components and direct tracer comparisons, MMII attempted to decouple the issues of transport and chemistry by use of tracer-tracer correlations and age of air calculations.

Twenty-nine models from all over the world, of which twelve were 2-D and seventeen were 3-D, participated to some degree in the MMII experiments. The eleven experiments, six related to transport and five to chemistry, were designed to try to identify and validate the various components which combine to give an accurate calculation of ozone concentration. AER participated fully in the MMII exercises, completing all 11 experiments. Dr. Malcolm Ko was a key contributor both to the development of the exercises and as a co-editor for many sections. AER (M. Ko and D. Weisenstein) acted as the definition lead for the "Prescribed Ozone P/L Chemistry Run", experiment B-3, and as the analysis lead (C. Scott and M. Ko) for the "Source Gas Comparison" exercise, as subset of experiment B-1.

Transport characteristics of the models were evaluated using simulations of the mean age of stratospheric air, its age spectrum, and the propagation of annually periodic oscillations originating at the tropical tropopause. These are compared with age of air derived from atmospheric observations of SF_6, CO_2, and H_2O. Large variations in transport are seen between models. These variations are evident both locally and globally. Most models that participated in the exercise have mean ages that are smaller than the observations suggest. Also, many of the models have unrealistic features in their mean age contour isopleths, suggesting that the tropical regions are not isolated enough. The model to model differences in transport can be seen in long-lived source gases, although the magnitude is reduced. This suggests that the variations in transport have a significant impact on the ability of the assessment models to predict the environmental impact of various perturbations, such as those due to HSCT emissions. Given the above and the fact that there is a positive correlation between mean age and the HSCT NO_y perturbation, many of the models may be underestimating the residence time of the HSCT emissions and their impact on ozone in the lower stratosphere.

The chemistry comparisons yielded more positive results. In general, the ozone comparisons above 25 km are good. Models tend to agree with each other and the measurements. In the region below 25 km, where heterogeneous chemistry and transport processes dominate, the models tend to diverge from the observations. However, in most cases, the partitioning of radical species within the NO_y, Cl_y, and Br_y families agrees well between models and with available observations. Most models underestimate the meridional gradient near the polar vortices, with 2-D and even 3-D models having a hard time accurately representing the PSC frequency of occurrence. Many of the calculated source gases and radical species from the models show a wide variation when compared to the measurements. In some cases, magnitudes of the species are comparable, but the seasonal cycles are not well represented. In other cases, the magnitudes vary widely.

AER performed the analysis for the "Source Gas Comparison" exercise and prepared the write-up on this section (reproduced here as ***Appendix J***) for the report. We examined 10 source gas species, emphasizing the link between the source gases and transport. The source species encompassed a range of global lifetimes from 2.5 years to 180 years. A comparative analysis of calculated stratospheric and global lifetimes was performed, along with analysis of concentration gradients at 75 and 10 mb, to try to determine how the transport of individual models can effect source gases. Based on our examination of the participating models, we found evidence that in the lower stratosphere a stronger tropical barrier will mean younger stratospheric lifetimes, higher source gas mixing ratios in the equatorial region and lower source gas mixing ratios in the midlatitudes. Models that tend to calculate shorter lifetimes have steeper latitudinal gradients. This may be indicative of the strength of the tropical upwelling and the permeability of the tropical barrier.

The differences in model-calculated lifetimes seems to be related to the age of air derived from SF_6 and other tracer experiments. Models that are calculating longer lifetimes tend to have older ages, giving model-calculated ages that are closer to the age of air derived from measurements of SF_6 and CO_2. Some of the model-calculated source gas lifetimes are longer than observations suggest, implying that the upwelling in the lower tropical stratosphere is too weak in those models. This is inconsistent with the conclusion from the CO_2 study, which shows that the model calculated seasonal signal for CO_2 is advected up in the tropics faster than observations. Calculated species cross sections of N_2O and CH_4 show larger gradients across the tropical barrier than the UARS data would indicate. Conversely, measurements of $CFCl_3$ from the ATMOS and ER-2 flights indicate a larger gradient at the 75 mb level than the models are exhibiting, indicating that the models may have too much meridional mixing at the 75 mb level. A large spread of calculated mixing ratio values is seen at high latitudes for all species examined. Based on the source gas analysis, many of the models are not doing a reasonable job in their transport.

VI. Climate Chemistry Interactions

VI.1 Model Description

The 2-D Interactive Climate-Chemistry Model (ICCM) is based on coupling two existing models (or ICCM modules) developed at AER: the refined seasonal-radiative-dynamical climate model (Wang et al., 1990; Molnar et al., 1994, and MacKay et al., 1997a) and the interactive chemistry-dynamics model (Ko et al., 1993 and Schneider et al., 1993).

The climate model and the chemistry model have the same meridional resolution, but different vertical coordinates. The climate module has better representation of the troposphere with finer tropospheric vertical resolution, more detailed atmospheric and surface physics, and separate land and ocean sectors in each zone. The chemistry-dynamics module has better representation of the stratosphere with finer stratospheric vertical resolution, and explicit calculation of heat transport and mean residual circulation. Because the physics and numerics of the two modules are different, we use a "modular" method to couple them. This method allows the two modules to run in parallel, and to exchange information continuously during long time integrations. Specifically, we use the chemistry module stratospheric temperatures and trace gas concentrations as input for the climate module during the time integration by replacing the stratosphere temperature field in the climate module by the temperature calculated from the chemistry-dynamics module. We also use the climate module tropospheric temperatures as input for the chemistry module. Since Newtonian cooling is used in the troposphere of the Schneider et al. (1993) chemistry-dynamics module, with climatological temperature (Cunnold et al., 1975) used as the "target" temperature, we use the temperature calculated from the climate module to replace the climatological "target" temperature. This is equivalent to forcing the tropospheric temperature gradually toward that calculated by the climate module. This data exchanging procedure provides the coupling of the two modules.

VI.2 Effects of Ozone Depletion on Climate

In order to study the potential climatic effects of the ozone hole more directly and to assess the validity of previous lower resolution model results, the latest high spatial resolution version of the AER seasonal radiative dynamical climate model is used to simulate the climatic effects of ozone changes relative to the other greenhouse gases. The steady state climatic effect of a sustained decrease in lower stratospheric ozone, similar in magnitude to the observed 1979 to 1990 decrease, is estimated by comparing three steady state climate simulations: 1) 1979 greenhouse gas concentrations and 1979 ozone; 2) 1990 greenhouse gas concentrations with 1979 ozone; and 3) 1990 greenhouse gas concentrations with 1990 ozone. The simulated

increase in surface air temperature resulting from non-ozone greenhouse gases is 0.272 K. When changes in lower stratospheric ozone are included, the greenhouse warming is 0.165 K which is approximately 39% lower than when ozone is fixed at the 1979 concentrations. Ozone perturbations at high latitudes result in a cooling of the surface-troposphere system that is greater (by a factor of 2.8) than that estimated from the change in radiative forcing resulting from ozone depletion and the model's $2xCO_2$ climate sensitivity. Our results suggest that changes in meridional heat transport from low to high latitudes combined with the decrease in the infrared opacity of the lower stratosphere are very important in determining the steady state response to high latitude ozone losses. The 39% compensation in greenhouse warming resulting from lower stratospheric ozone losses is also larger than the 28% compensation simulated previously by the lower resolution model. The higher resolution model is able to resolve the high latitude features of the assumed ozone perturbation which are important in determining the overall climate sensitivity to these perturbations.

This work appeared in the Journal of Climate (MacKay et al., 1997 see ***Appendix K***).

VI.3 Stratospheric Cooling and Arctic Ozone Recovery

Realization of the Montreal Protocol curbing the CFCs emissions is believed to reduce the chlorine loading of the atmosphere in the next century. However, concerns still remain whether this measure is sufficient to avoid further ozone depletion, particularly in the densely populated areas in the Northern hemisphere. This concern is especially valid, since it is accepted now that future colder stratospheric conditions due to greenhouse gas emissions could facilitate formation of the polar stratospheric clouds (PSCs) (e.g., WMO, 1999; Shindell et al., 1998).

The purpose of our study was to investigate the ozone behavior along a typical idealized air parcel in the Arctic stratosphere under projected declining chlorine loading superimposed with assumed temperature trends. We explore the chemical implications of the stratospheric cooling assuming the same air parcel trajectory and ignoring ozone radiative and dynamical feedbacks.

Details of our calculations are presented in Danilin et al. (1998) (see **Appendix L**). Briefly, we initialize our model at 70°N based on the climatological values according to the UARS measurements and make calculations from December 1 to April 1 along a typical air parcel finishing at 50 mb. Effects of stratospheric cooling on the ozone content are investigated by homogeneous reduction of the temperature along this parcel. Since the formation of the type I PSCs is still a subject for discussion, we present results for the nitric acid trihydrate (NAT) and supercooled ternary solution (STS) PSC schemes. Figure VI.1 shows the sensitivity of the maximum ozone depletion along this parcel (occurred on April 1 and expressed in % from its

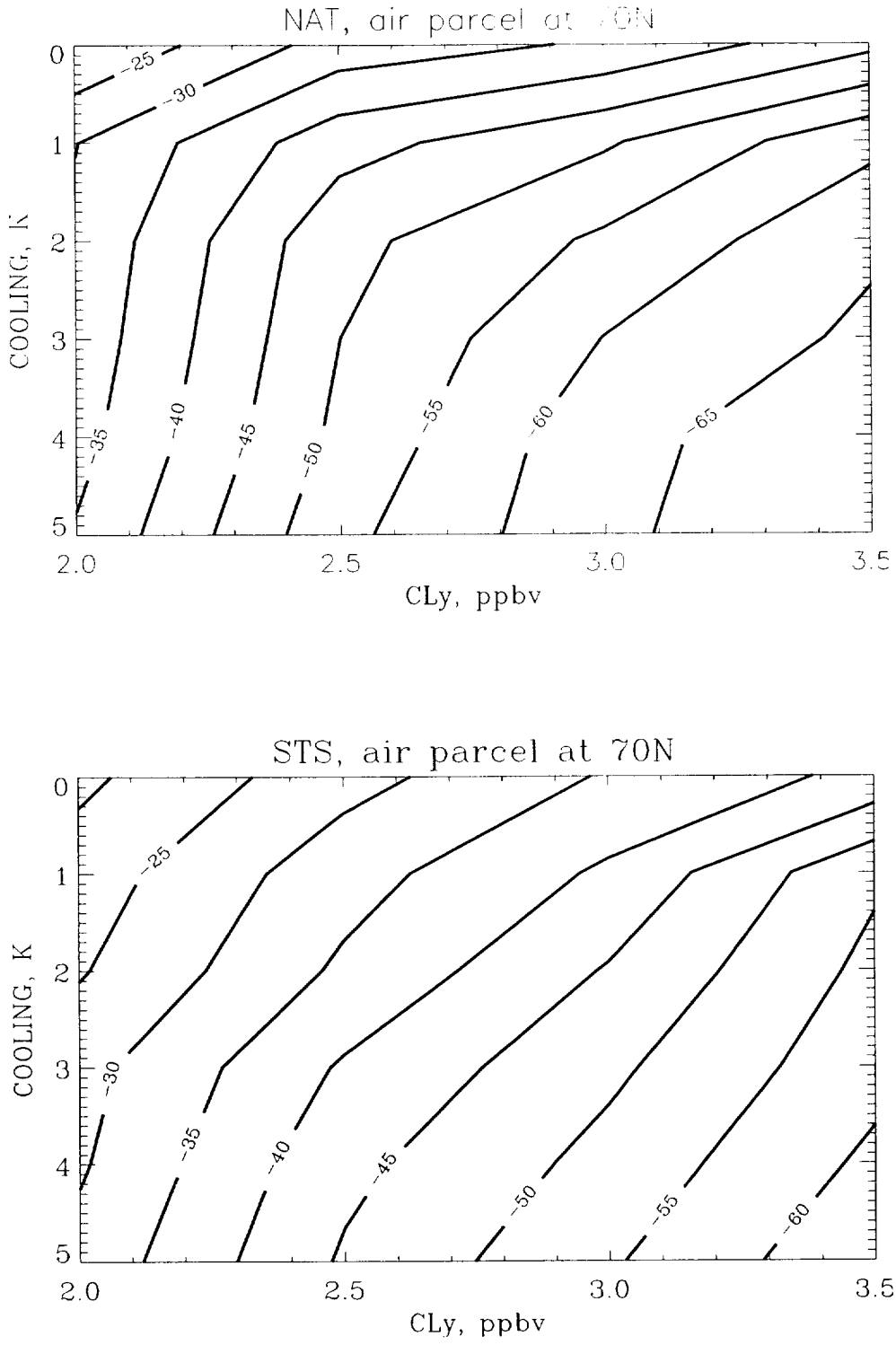

Figure VI.1 Isolines of ozone change in the air parcel on April 1 (in % of initial 3.6 ppmv) as a function of chlorine loading and stratospheric cooling at 20 km altitude for the NAT (top) and STS (bottom) schemes. Details of the model runs are given in Danilin et al. (1998).

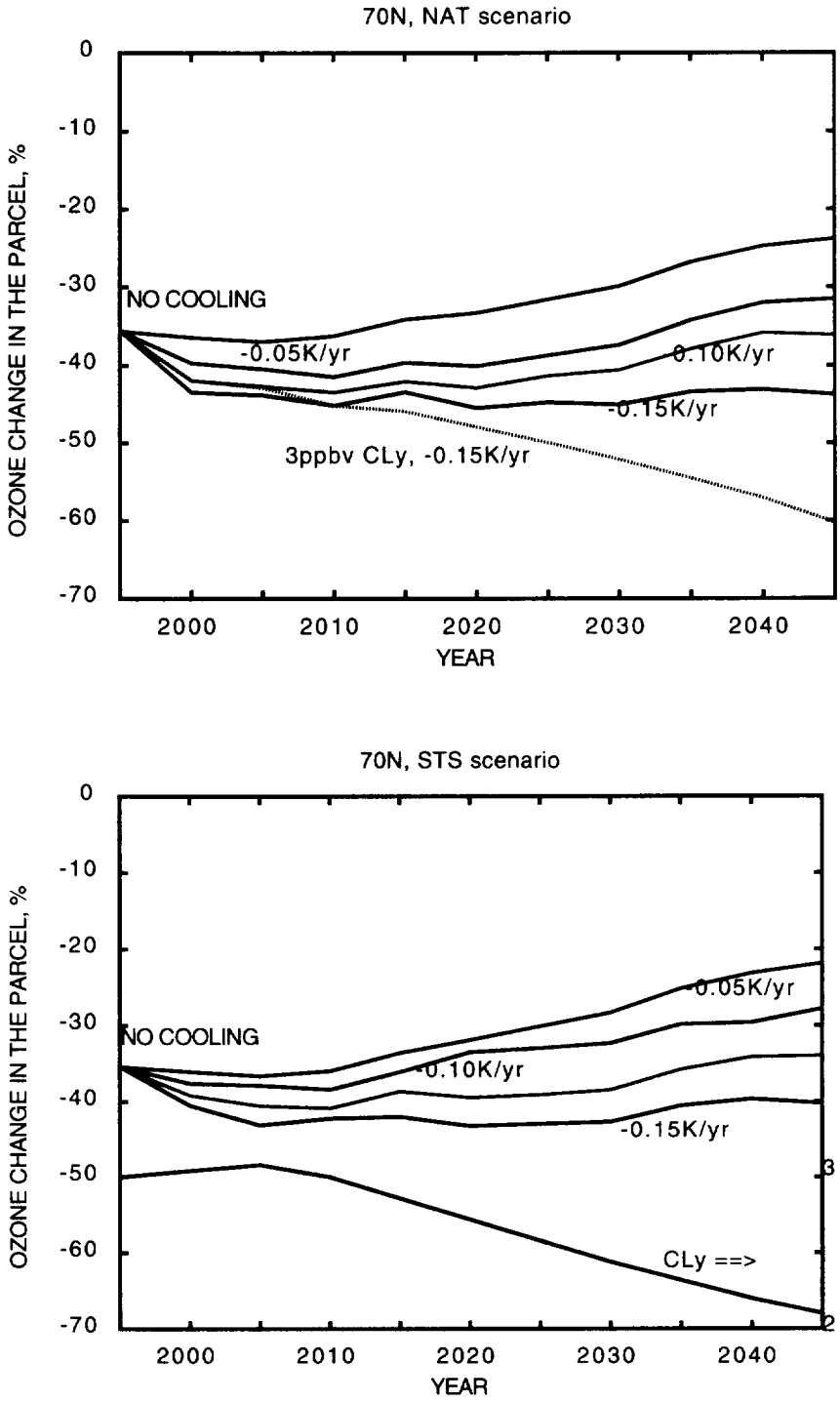

Figure VI.2 Ozone depletion for the NAT (top) and STS (bottom) PSC schemes as a function of year for the projected chlorine loading and different temperature trends.

initial value of 3.6 ppmv) as a function of chlorine loading and stratospheric cooling for the NAT and STS PSC schemes. We introduce a chlorine-cooling equivalent, which numerically is equal to the slope of these isolines in a point of interest. For example, for the current conditions a 1 K cooling produces the same effect on the local ozone content as 0.4 (0.7) ppbv increase in chlorine loading for the STS (NAT) scheme.

If we consider the projected evolution of the chlorine loading and extrapolated the observed temperature trends in the lower stratosphere (WMO, 1999) for the next 50 years, the ozone recovery calculated is shown in Figure VI.2. Our results clearly show that possible stratospheric cooling could indeed cause a delay in the ozone recovery up to 10-20 years depending on the scenario. Thus, accurate prediction of the ozone behavior under the fragile Arctic conditions requires more detailed studies of the reasons for the lower stratospheric cooling with all necessary feedbacks.

VI.4 AER 3-wave Interactive Model and Climate-chemistry Coupling

Most 2-D stratospheric CTMs used for the ozone assessment and global change studies have fixed dynamics, i.e. the temperature, the circulation, and the eddy diffusion are prescribed parameters. These parameters are selected to well represent the atmosphere for a special year or more commonly, the climatology of the atmosphere. However, any perturbations in ozone or other radiatively-active components of the atmosphere would change the dynamics of the atmosphere through the couplings between the chemical, radiative and dynamical processes. If the perturbations are grave enough, the fixed dynamics of 2-D CTM may not be consistent with the chemical composition of the perturbed atmosphere and, therefore, could lead to incorrect simulation of distribution for ozone and other tracers. We have observed this kind of perturbations after huge volcanic eruptions, in QBO, or during solar variations, and very likely will see them when the CO_2 is doubled in the middle of the next century or when the High Speed Civil Transport (HSCT) fleet is deployed early next century. The 2-D interactive model is design to solve this problem. By coupling the 2-D CTM with the dynamics model, the dynamics is consistent with distributions of ozone and other radiatively-active chemical components of the atmosphere. AER developed a 2-D interactive model (Ko et al., 1993) and used it to assess the ozone response to the increases of greenhouse gases (Schneider et al., 1993). Although the circulation and temperature used in the transport of chemical species are calculated in the AER 2-D interactive model, the eddy diffusion coefficients are still prescribed. They are adjustable parameters and are not necessarily consistent with modeled ozone distribution. Therefore, the interactions between the dynamics and chemistry are inadequate. The AER 3-wave model is modified to remedy this deficiency of the AER 2-D interactive model. It couples a semi-spectral dynamics model, a radiative transfer code and a comprehensive 2-D chemistry transport model. The semi-spectral dynamics model integrates the primitive equations for zonal mean and three longest zonal waves of dynamical variables. The wave breaking parameterization (Garcia, 1991) is implemented in the model. When the amplitudes of waves grow to exceed the zonal mean, a damping term is introduced into the wave equations to keep the wave amplitudes below the zonal mean values. The damping also creates a strong wave mixing in the transport for chemical components of the atmosphere. This parameterization has been successfully used in several models (Garcia et al., 1992; Garcia and Solomon, 1994; Kinnersley, 1995). The residual circulation used in the tracer transport is calculate from the zonal means and the longest 3 zonal waves of the velocity and geopotential, which are integrated in the semi-spectral dynamics model. Also, the simulated ozone distributions are used in the net heating calculation. Thus, the 3-wave model includes most interaction mechanisms between the chemical, radiative and dynamical processes in the stratosphere.

The eddy diffusion consists of two parts, the chemical eddy diffusion and the mixing by the planetary wave breaking. It is found that for ozone and most other long-lived tracers the chemical eddy diffusion is negligible compared to the wave mixing. It is also found that compared with the values commonly used in 2-D CTMs, the eddy diffusion coefficients in the 3-wave model generally are smaller. This is more so in the tropics of the stratosphere, which is similar to the 2-D CTM with a tropical pipe (Weisenstein et al., 1996). The model has been used to simulate the present day atmosphere. A reasonable agreement between the model simulation and observations is reached in dynamical variables and in the distribution of tracers like ozone, N_2O and CH_4 (see ***Appendix M***).

In order to investigate the interactions between the chemistry and dynamics, especially the feedback of ozone changes, the 3-wave model is used to simulate the atmospheric effects of engine emissions from HSCT fleet, which has 500 supersonic airplanes with Mach=2.4 and NO_x emission index, EI=15. From the 3-wave simulations we find:

a. Ozone depletion caused by HSCT engine emissions in the northern mid- and high-latitudes is significantly larger in 3-wave model simulations than in that of the AER 2-D CTM. In the tropics, HSCT engine emissions increase the ozone column abundance in 3-wave model simulations. This character is also found in the results of the AER 2-D CTM with the tropical pipe.

b. The differences of the ozone depletion caused by HSCT engine emissions between 3-wave model and the AER 2-D CTM are largely due to the different transports for ozone, not the differences in the distributions of the engine emissions in two models.

c. The feedback of ozone changes through changes in the dynamics simulated by the 3-wave model alters the ozone response to the HSCT engine emissions. The feedback is a negative one. This means the feedback remedies part of the damage of the HSCT emissions. The feedback reduces the ozone depletion in northern midlatitudes by 20%-30%, mainly by the ozone feedback through changes in the circulation.

The details of model results can be found in the ***Appendix N***.

VII. Age of Air

Hall and Plumb (1994) introduced the concept of the age spectrum and used model simulated distributions of artificial tracers to obtain estimates of stratospheric mean age of air. The content of a unit element of air at a particular location and particular time of year in the stratosphere can be thought of as a mixture of different air parcels that have taken different routes to arrive at that location. The mean age of air at that location and time ($\Gamma(x,t)$, where t is time of the year) is defined as the average transit times of the air parcels since their last contacts with the tropopause. Although it is difficult to isolate the effects of $\Gamma(x,t)$ on calculated concentrations of photochemically-active species, it provides one way to objectively quantify transport rates in different models. Hall and Plumb also showed that $\Gamma(x,t)$ is related to the local concentration of an inert trace gas at location x and time t provided that the tracer gas has an approximately linearly increasing tropospheric concentration and has had sufficient time to accumulate in the atmosphere. If such a tracer is present in the atmosphere, the measured concentrations of this tracer can be used to derive an empirical mean age, $\Gamma_{obs}(x,t)$, for the atmosphere to verify model results. Sulfur hexafloride (SF_6) has a long lifetime, ~3200 years (Ravishankara et al., 1993) and has been identified (Elkins et al., 1996) as an ideal tracer for deriving $\Gamma_{obs}(x,t)$.

VII.1 Utilizing SF_6 Data from the POLARIS Campaign

Through our participation in the POLARIS campaign, we have the opportunity to work with Dr. Elkins to use the SF6 data from his group and his method to derive the age of air from observed SF_6 concentration. In this study, we discuss the mean age of air calculated using different methods and different versions of the AER 2-D Chemistry Transport Model (CTM) and compare the results with $\Gamma_{obs}(x,t)$ derived from the SF_6 measurements. Variations between models and even different calculations using the same model may calculate different mean ages of air. We obtain $\Gamma(x,t)$ by simulating the concentration of SF_6 using historical boundary conditions and by calculating a pseudo tracer as defined by Boering et al. (1996). In our sensitivity studies, we have found that weaker upwelling in the tropics increases the stratospheric age of air significantly. However, these changes in the AER 2-D circulation also made the lifetimes of many of the long-lived source gases longer than observations would suggest. Due to these findings, we feel that mean age should not be used as the sole criteria for judging transport rates in models. A paper has been prepared and is being reviewed by the co-authors. It will be submitted for review soon. A copy of the manuscript is included as ***Appendix O***.

VII.2 Sensitivity of Model Calculated Age to Removal of SF_6 in the Mesosphere

The AER 2-D chemistry and transport model only covered the region from the surface up to about 60 km. The top of the model is closed. It means there are no exchanges or interactions across the top of the model. This is a good approximation for most applications of 2-D CTM, e.g. ozone assessment, because ozone density is extremely low already in the upper stratosphere due to photochemical reactions. However, the sink in the mesosphere or above could effect the distribution in the upper stratosphere of species, which doesn't have sink there. We have used the AER 2-D CTM with fine vertical resolution (1.2 km) and put a sink in the top layer to simulate the sink above for SF_6. The specified strength of the sink creates a lifetime of about 3000 years for SF_6. We find the derived age of air increases from less than 4 years to longer than 6 years in the upper stratosphere. However, when we spread the sink into the top four layers, the changes in the age of air are reduced considerably. This may explain the contradiction between our results and that of Hall and Waugh (1998).

VII.3 Sensitivity of Model Calculated Age to Transport Circulation

The sensitivity of the age of air calculations to the choice of the transport circulation has been tested using the streamfunctions discussed in Section I.2.c: MLS-92, MLS-93, CLAES-92, NCEP, and GSFC. The resulting age of air (AOA) distributions, computed using the standard set of horizontal and vertical diffusion coefficients from the AER model, are shown in Figure VII.1. It is clear that all distributions are too young, especially in the upper stratosphere, where the measurements indicate ages as old as 10 years (Harnish et al., 1999). There is some variation among the different distributions, e.g., the MLS-92 streamfunction leads to somewhat older ages than the other circulations. We note, however, that this particular streamfunction is almost certainly unrealistic, in view of the problems with the MLS measurements early in the UARS mission. These problems include a low bias in the ozone measurements at 46 hPa in the tropics (and an associated slow bias in the diagnosed circulation) as well and a cold bias in the temperature fields adopted in the MLS version 3 files (which again leads to an overly sluggish circulation diagnosed from heating rates based on these temperatures). After experimenting with various combinations of streamfunctions and diffusion coefficients, we have determined that the young bias can only be eliminated by adopting large values for the horizontal diffusion coefficients K_{yy}. This is illustrated in Figure VII.2, which shows AOA distributions computed using the MLS-92 streamfunction and two sets of K_{yy}s: the standard values from the "pipe" version of the AER circulation and the uniform values of 10^{10} cm^2s^{-1}. Rapid horizontal mixing

results in significantly older ages, by allowing air to recirculate the stratosphere more times before being flushed out into the troposphere (Neu and Plumb, 1999).

While values of K_{yy} as large as 10^{10} cm^2s^{-1} seem unrealistic, this could only be determined by inspecting the distributions of tracers affected by chemistry, such as ozone. As a matter of fact, the standard diagnostic of this kind, the column ozone, shows remarkably little sensitivity to the adoption of large K_{yy}s. The distributions of other constituents can be more strongly affected by the horizontal mixing, but we note that using chemical species to assess the realism of a particular set of K_{yy} is inconsistent with the notion of age as a diagnostic of transport unaffected by chemical parameterizations. In other words, AOA calculations alone are insufficient to validate a particular transport circulation in a 2-D model. The concept of age may be better suited as a transport diagnostics in 3-D models, but in those models the age distributions can be extremely sensitive to the numerical aspects of the calculations, such as the choice of advection and time-stepping schemes (Eluszkiewicz et al., 1999). In a 2-D model, these numerical aspects are unimportant, owing to the presence of parameterized diffusion (i.e., K_{yy}) and the smooth nature of the monthly-varying circulation. We have carried out AOA calculations with a variety of advection schemes (including centered-difference, upstream, and the second-moment schemes) and have indeed determined that, with the same streamfunction and diffusion coefficients, the resulting AOA distributions are indistinguishable from one another.

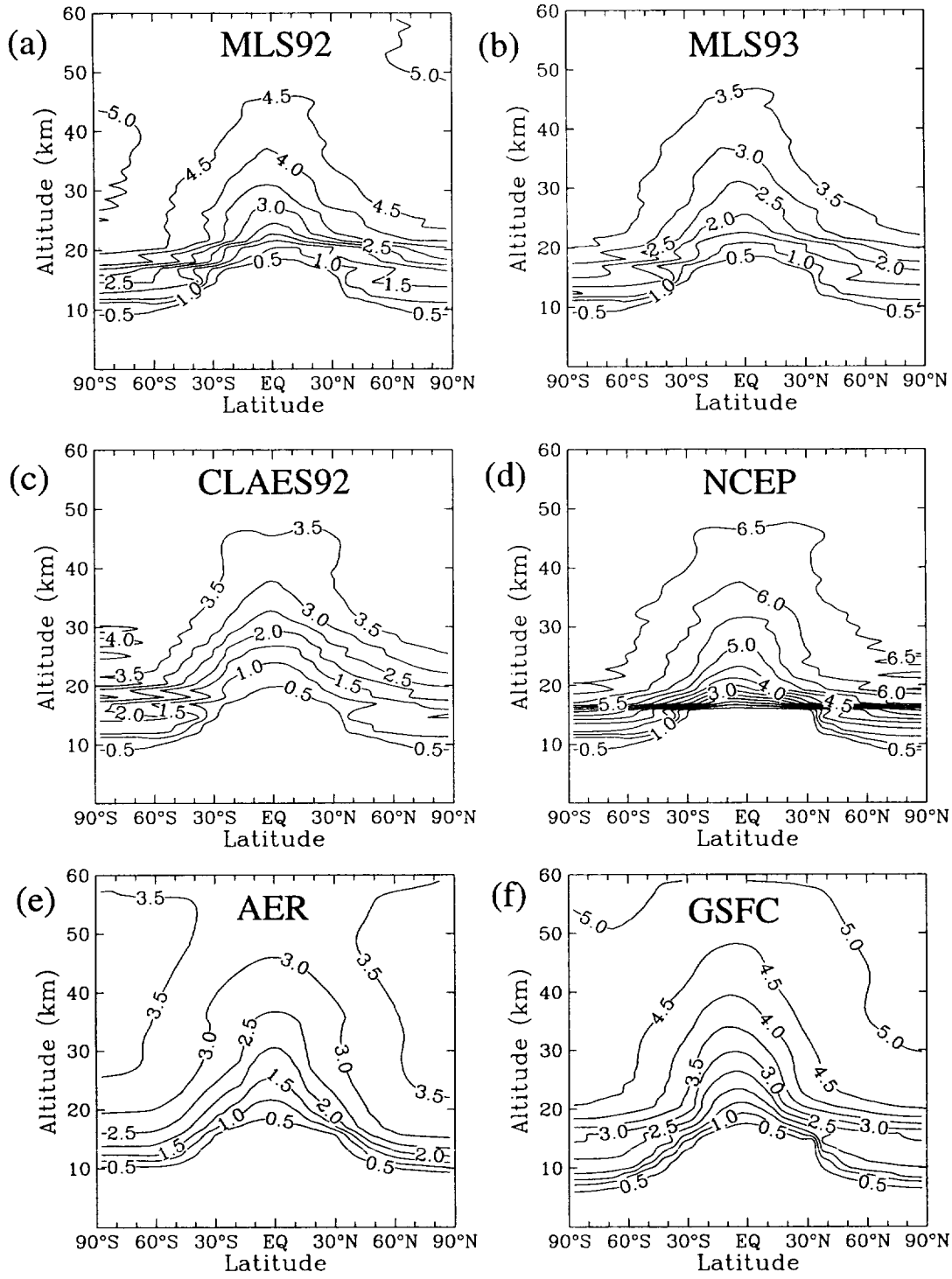

Figure VII.1 Sensitivity of 2-D age of air calculations to the choice of streamfunction: (a) MLS-based streamfunction for 1992, (b) MLS-based streamfunction for 1993, (c) CLAES-based streamfunction for 1992, (d) NCEP streamfunction, (e) standard AER streamfunction, and (f) GSFC streamfunction. See section I.2.c for details.

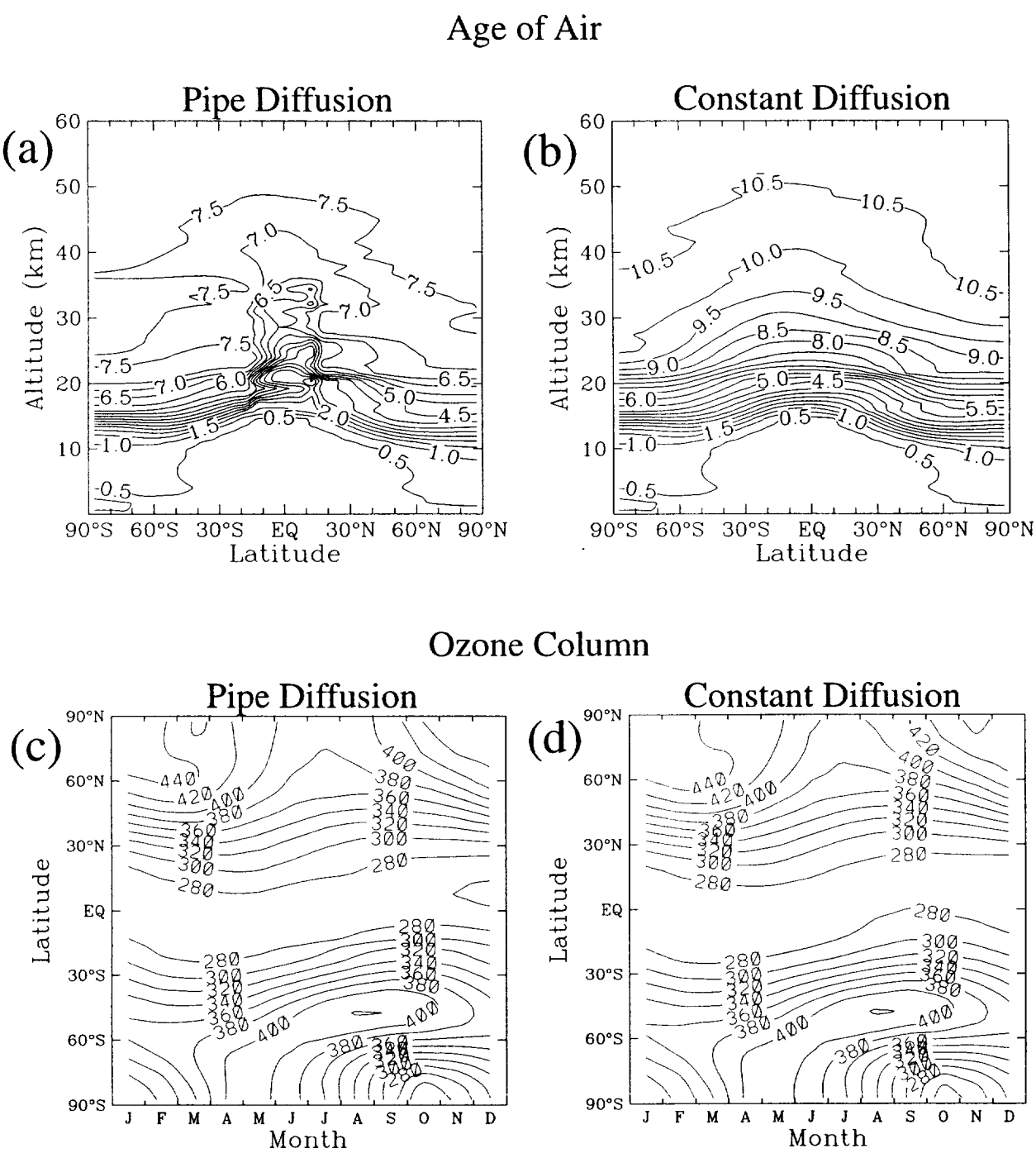

Figure VII.2 Effect of horizontal diffusion on the age of air calculations: (a) age with "pipe" K_{yy}s, (b) age with $K_{yy} = 10^{10}$ cm^{2}s^{-1}, (c) O_3 column with "pipe" K_{yy}s, and (d) O_3 column with $K_{yy} = 1010$ cm^{2}s^{-1}. The MLS-1992 streamfunction has been used in both cases. Ages are shown in years and O_3 column in dobson units.

VIII. Modeling Studies Using 3-D CTM

Currently, 2-D CTMs are the standard tool for HSCT ozone assessment and global changes in the stratosphere provoked by anthropogenic or natural perturbations. Because atmospheric transport is three-dimensional (3-D) in nature, 3-D CTMs are more realistic than 2-D CTMs to investigate these problems. A new focus on understanding ozone change is the possible impact from transport of radicals and short-lived trace gases from the troposphere to the stratosphere (Ko et al., 1998). This pathway of supplying radicals to the stratosphere is not well represented in 2-D models. Thus, one would need to use a 3-D model with parameterization for convective transport. Even in the stratosphere, if the perturbation is zonally asymmetric, e.g. the emissions from the space shuttles, 3-D CTM is more relevant.

Through our collaboration with Professor Michael Prather of UC Irvine, we were given access to the 8°x10° versions of the GISS/Harvard/UCI 3-D CTM for the troposphere and the stratosphere. The tropospheric version has 9 vertical layers, which cover from the surface to 10 mb, and the stratospheric version has 21 layers, which extend to 0.002 mb. The model is driven by a set of dynamical fields, which are generated by the GISS GCM. They include 3-D wind, temperature and convection statistics. For the stratospheric version, the data are recorded every 8 hours and the tropospheric version, every 4 hours. The data of one year from GISS GCM output are used in 3-D CTM repeatedly for multiyear runs.

The transport of the 3-D CTM has been extensively tested previously. The cross-tropics transport has been examined by comparing the model simulations with measurements of long-lived fluorocarbons, CH_3CCl_3 and ^{85}Kr (Prather et al., 1987; Jacob et al., 1987). The vertical transport by convection was tested through comparisons to ^{222}Rn measurements (Jacob and Prather, 1990).

We modified the GISS/Harvard/UCI 3-D CTM and used the model to perform the following studies:

1. to predict the accumulation of trifluoroacetic acid from degradation of HFC in the atmosphere using the tropospheric version of the model,

2. to study the atmospheric mercury budget, giving deposition rates from current emissions, also using the tropospheric version of the model,

3. to study the distribution of aluminum oxide particles from solid rocket exhaust associated with the Space Shuttle and Titan launches using the stratospheric version of the model.

VIII.1 Degradation of HCFCs and HFCs

The long-lived fully halogenated organic compounds are being replaced by HCSCs and HFCs. This is becausee smaller atmospheric accumulations for these chemicals are expected due to removal by reactions with OH in the troposphere, leading to smaller ozone depletion potential and global warming indicies. However, the acceptability of HCFCs/HFCs also pertains to the impact of these componds or their degradation products on econsystem.

Trifluoroacetic acid (TFA, CF_3COOH) is produced by the degradation of the halocarbon replacements HFC-134a, HCFC-124 and HCFC-123 in the clouds. It is finally deposited onto the surface by washout or dry deposition. Concern has been raised about the possible long-term accumulation of TFA in certain aquatic environments. The GISS/Harvard/UCI 3-D CTM has been modified to include the parameterizations for washout and dry deposition and to add a chemistry module for the degradation of HFC/HCFC. The model simulated the HFC/HCFC precursors of TFA that include the rates of formation and global deposition of TFA based on assumed future emissions. The highest monthly averaged rainwater concentrations of TFA for northern midlatitudes were calculated for the month of July, corresponding to 0.3-0.45 μg/L in parts of North America and Europe in the year 2010. The model results are sensitive to the parameterization of rainout, cloud cover, OH concentration, TSA cloud residence time and TFA yield. Our simulations also show the crucial role played by long-range transport of gas phase TFA in smoothing out the chemical impact of asymmetries in the OH and rainfall fields. The detailed analyses of the model simulations and discussions can be found in ***Appendix P***.

VIII.2 Global Simulation of Atmospheric Mercury

After being emitted into the atmosphere, Mercury (Hg) can be transported over long distances before being deposited through precipitation or dry processes back to the earth's surface. It can enter the aquatic food chain in surface water bodies and biologically accumulate in fish to high trophic level. High consumption of fish with high levels of Hg may lead to potential health hazards for humans and ecological impacts on wildlife. Therefore, to assess the possible impacts of Hg emissions on the environment, it is essential to understand the atmospheric processes that govern the transport, chemical transformations, and deposition processes in the atmosphere.

The parameterization of wet and dry deposition for Hg compounds and a module for Hg gaseous and aqueous chemistry are implemented into the framework of GISS/Harvard/UCI 3-D CTM. The natural and anthropogenic Hg surface emission sources of 4,000 Mg/y and 2,100 Mg/y, respectively, are used as input to the model. The model simulates their long-range

transport, chemical transformations and finally depositions back to the earth surface of Hg. The model simulations show that the deposition on land surfaces accounts for 47% of total global deposition. The simulated Hg ambient surface concentrations and deposition fluxes to the earth's surface are consistent with available observations. Observed spatial and seasonal trends are reproduced by the model although larger spatial variations are observed in Hg(0) surface concentrations than predicted by the model. The calculated atmospheric residence time of Hg is about 1.7 year. Chemical transformations between Hg(0) and Hg(II) have a strong influence on Hg deposition patterns, because Hg(II) is removed faster than Hg(0). Oxidation of Hg(0) to Hg(II) occurs primarily in the gas phase whereas Hg(II) reduction to Hg(0) occurs solely in the aqueous phase. When only gas-phase chemistry of Hg is simulated, the atmospheric residence time is reduced to 1.2 year and the Hg(0) concentrations are lower by 0.8 ng/m^3 due the absence of the Hg(II) reduction pathway. This result suggests that aqueous chemistry is an essential component of the atmospheric cycling of Hg. For more details of this study, please see ***Appendix Q***.

VIII.3 Global Impact of Solid Rocket Motor Launchers

Recent laboratory measurements (Molina et al., 1997) have indicated that the heterogeneous chlorine activation reaction $ClONO_2 + HCl \rightarrow HNO_3 + Cl_2$ has a reaction probability of about 0.02 on aluminum oxide particles. This may impact stratospheric ozone layer. A similar reaction on PSCs and sulfate aerosols is believed to be responsible for much of the Arctic and Antarctic ozone loss in springtime. Heterogeneous reaction on Al_2O_3 particles would not be limited to the polar region like the similar reaction on PSCs, because the reaction rate is not temperature-dependent. It also could occur at all latitudes and seasons. The impact of the Al_2O_3 particulate from Solid Rocket Motor (SRM) on ozone was studied using GISS/Harvard/UCI 3-D model and the AER 2-D CTM. The stratospheric version of GISS/Harvard/UCI 3-D model was modified by adding sedimentation and removal through collision with background sulfate aerosols for Al_2O_3 particulate. Since the rates of sedimentation and collision removal are size-dependent, Al_2O_3 particles are grouped into 13 bins according to their size and every bin of particles is transported independently in the 3-D model. The yearly sources for each bin of the Al_2O_3 particles from launches of the Space Shuttles and Titan are input into the 3-D model. The final distribution of the surface area for all bins are added up to give the total surface area distribution of Al_2O_3 particles. The zonal average of this 3-D distribution of surface area is used in the AER 2-D CTM to assess the impact of the Al_2O_3 particulate.

It is found that even ignoring the sedimentation and the collision removal, the impact of Al_2O_3 particulate to the stratospheric ozone is much less important than the background sulfate aerosols. This is because the total source of Al_2O_3 particles is too small (1120 ton/yr). For more details about this research, please see ***Appendix R***.

IX. Publications

Transport in the stratosphere

Keim, E. et al. (1997), Measurements of NO_y-N_2O correlation in the lower stratosphere: latitudinal and seasonal changes and model comparisons, *JGR*, **102**, 13193-13212.

Shia, R.-L., M.K.W. Ko, D.K. Weisenstein, C. Scott, and J. Rodriguez (1998), Transport between the tropical and mid-latitude lower stratosphere: Implication for ozone response to HSCT emissions, *J. Geophys. Res.*, **103**, 25435-25446.

Chlorine/bromine loading

Ko, M.K.W., N.-D. Sze, C. Scott, and D.K. Weisenstein (1997), On the relation between stratospheric chlorine/bromine loading and short-lived tropospheric source gases, *J. Geophys. Res.* **102**, D21, 25507-25517.

Wamsley, P.R. et al. (1998), Distribution of halon-1211 in the upper troposphere and lower stratosphere and the 1994 total bromine budget, *JGR*, **103**, 1513-1526.

Chemistry partitioning

Gao et al., (1999), A comparison of observations and model simulations of NO_x/NO_y in the lower stratosphere, *Geophys. Res. Lett.*, **26**, 1153-1156.

Danilin, M. et al., (1999), Nitrogen species in the post-Pinatubo stratosphere: Model analysis utilizing UARS measurements, *J. Geophys. Res.*, **104**, 8247-8262.

Ozone Assessment

McCall, D.W. et al., (1997), *Fire Suppression Substitutes and Alternatives to Halon for U.S. Navy Applications*, Committee on Assessment of Fire Suppression Substitutes and Alternatives to Halon, Naval Studies Board, Commission on Physical Sciences, Mathematics, and Applications, National Research Council, National Academy Press, Washington, D.C.

Ko, M.K.W., N.D. Sze, C. Scott, J.M. Rodriguez, and D.K. Weisenstein, (1998) Ozone depletion potential of CH_3Br, *J. Geophys. Res.*, **103**, 28187-28195.

Isaksen, I., et al. (1999), "Modeling the Chemical Composition of the Future Atmosphere", *in IPCC Special Report on Aviation and the Global Atmosphere.*

Prinn et al. (1999), "Long-lived Ozone-related Compounds" in *Scientific Assessment of Ozone Depletion: 1998*, World Meteorological Organization Global Ozone Research and Monitoring Project, report No. 44. Geneva, Switzerland.

Kurylo, M.J. and J.M. Rodriguez (1999) "Short-lived ozone-related compounds" in *Scientific Assessment of Ozone Depletion: 1998*, World Meteorological Organization Global Ozone Research and Monitoring Project, report No. 44. Geneva, Switzerland.

Ozone/climate coupling

MacKay, R.M., M.K.W. Ko, S. Zhou, G. Molnar, R.-L. Shia, Y. Yang, (1997) An estimate of the climatic effect of ozone during the 1980s. *J. of Climate*, **10**, 774-788.

Danilin, M.Y., N.-D. Sze, M.K.W. Ko, J.M. Rodriguez and A. Tabazadeh, (1998) Stratospheric cooling and Arctic ozone recovery, *GRL*, **25**, 2141-2144.

Studies using the GISS 3-D model

Kotamarthi, V.R., J.M. Rodriguez, M.K.W. Ko, T.K. Tromp, N.-D. Sze (1998) Trifluoroacetic acid from the degradation of HCFC and HFCs: a three dimensional modeling study, *J. Geophys. Res.* **103**, 5747-5758.

Shia, R.-L., C. Seigneur, P. Pai, M. Ko, and N.-D. Sze (1999) Global Simulation of Atmospheric Mercury Concentrations and Deposition Fluxes, *J. Geophys. Res.*, in press.

References

Boering, K.A., S.C. Wofsy, B.C. Daube, H.R. Schneider, M. Loewenstein, J.R. Podolske, T.J. Conway, Stratospheric Mean Ages and Transport Rates from Observations of Carbon Dioxide and Nitrous Oxide, *Science, 274*, 1340-1343, 1996.

Brown, S.S., et al., Rate constant for the reaction $OH + NO_2 + M \rightarrow HNO_3 + M$ under atmospheric conditions, *Che. Phys. Lett., 299*, 277, 1999a.

Brown, S.S, et al., Reconsideration of the rate constants for the reaction of hydroxyl radicals with nitric acid vapor, *J. Phys. Chem., 103*, 3031-3037, 1999b.

Burkholder, J.B., R.R. Wilson, T. Gierczak, R. Talukdar, S.A. McKeen, J.J. Orlando, G.L. Vaghjiani, and A.R. Ravishankara, Atmospheric fate of CF_3Br, CF_2BR_2, CF_2ClBr, and CF_2BrCF_2Br, *J. Geophys. Res., 96*, 5025-5043, 1991.

Butler, J.H., S.A. Montzka, A.D. Clarke, J.M. Lobert and J.W. Elkins, Growth and distribution of halons in the atmosphere, *J. Geophys. Res., 103*, 1503-1511, 1998.

Cunnold, D., F. Alyea, N. Phillips, and R.N. Prinn, A three-dimensional dynamical chemical model of atmospheric ozone. *J. Atmos. Sci., 32*, 170-194, 1975.

Cunnold, D.M., R.F. Weiss, R.G. Prinn, D. Hartley, P.G. Simmonds, P.J. Fraser, B. Miller, F.N. Alyea and L. Porter, GAGE/AGAGE measurements indicating reductions in global emissions of CCl_3F and CCl_2F_2 in 1992-1994, *J. Geophys. Res., 102*, 1259-1269, 1997.

Danilin, M.Y., N.-D. Sze, M.K.W. Ko, J.M. Rodriguez and A. Tabazadeh, Stratospheric cooling and Arctic ozone recovery, *GRL, 25*, 2141-2144, 1998.

Danilin et al., 1999, Nitrogen species in the post-Pinatubo stratosphere: Model analysis utilizing UARS measurements, *J. Geophys. Res., 104*, 8247-8262, 1999.

DeMore, W.B., S.P. Sander, D.M. Golden, R.F. Hampson, M.J. Kurylo, C.J. Howard, A.R. Ravishankara, C.E. Kolb, and M. J. Molina, Chemical kinetics and photochemical data for use in stratospheric modeling, *JPL Publ. 94-26*, 1994.

DeMore, W.B., S.P. Sander, D.M. Golden, R.F. Hampson, M.J. Kurylo, C.J. Howard, A.R. Ravishankara, C.E. Kolb, and M.J. Molina, Chemical kinetics and photochemical data for use in stratospheric modeling, *JPL Publ. 97-04*, 1997.

Donahue, N.M., M. Dubey, R. Mohrschladt, K.L. Demerjian and J.G. Anderson, A high pressure flow study of the reactions of $OH+NO_x \rightarrow HONO_x$: Errors in the falloff region, *J. Geophys. Res., 102*, 6159-6168, 1997.

Dransfield, T.J., K.K. Perkins, N.M. Donahue, J.G. Anderson, M.M. Sprengnether, and K.L. Demerjian, Temperature and pressure dependent kinetics of the gas-phase reaction of the hydroxyl radical with nitrogen dioxide, Geophys. Res. Lett., 26, 687-690, 1999.

Elkins, J.W., D.W. Fahey, J.M. Gilligan, G.S. Dutton, T.J. Baring, C.M. Volk, R.E. Dunn, R.C. Myers, S.A. Montzka, P.R. Wamsley, A.H. Hayden, J.H. Butler, T.M. Thompson, T.H. Swanson, E.J. Dlugokencky, P.C. Novelli, D.F. Hurst, J.M. Lobert, S.J. Ciciora, R.J. McLaughlin, T.L. Thompson, R.H. Winkler, P.J. Fraser, L.P. Steele, M.P. Lucarelli, Airborne gas chromatograph for in situ measurements of long lived species in the upper troposphere and lower stratosphere, *Geophys. Res. Lett., 23*, 347-350, 1996.

Eluszkiewicz, J., D. Crisp, R. Zurek, L. Elson, E. Fishbein, L. Froidevaux, J. Waters, R.G. Grainger, A. Lambert, R. Harwood, and G. Peckham, Residual circulation in the stratosphere and lower mesosphere as diagnosed from Microwave Limb Sounder data, *J. Atmos. Sci., 53*, 217-240, 1996.

Eluszkiewicz, J., D. Crisp, R.G. Grainger, A. Lambert, A.E. Roche, J.B. Kumer, and J.L. Mergenthaler, Sensitivity of the residual circulation diagnosed from the UARS data to the uncertainties in the input fields and to the inclusion of aerosols, *J. Atmos. Sci., 54*, 1739-1757, 1997.

Eluszkiewicz, J., R.S. Hemler, J.D. Mahlman, L. Bruhwiler, and L. L. Takacs, Sensitivity of age-of-air calculations to the choice of advection scheme. J. Atmos. Sci., 1999 (submitted).

Fahey, D.W., et al., *In situ* measurements constraining the role of sulfate aerosols in midlatitude ozone depletion, *Nature, 363*, 509-514, 1993.

Fleming, E.L., C.H. Jackman, R.S. Stolaski, and D.B. Considine, Simulations of stratospheric tracers using an improved empirically based two-dimensional model transport formulation, *J. Geophys. Res.*, 104, 23,911-23,934, 1999.

Gao et al., A comparison of observations and model simulations of NO_x/NO_y in the lower stratosphere, *Geophys. Res. Lett., 26*, 1153-1156, 1999.

Garcia, R.R., Parameterization of planetary wave breaking in the middle atmosphere. *J. Atmos. Sci., 48,* 1405-1419, 1991.

Garcia, R.R., and S. Solomon, A numerical model of the middle atmosphere 2. Ozone and related species. *J. Geophys. Res., 99,* 12,937-12,951, 1994.

Garcia, R.G., F. Strobel, S. Solomon, and J.T. Kiehl, A new numerical model of the middle atmosphere 1. Dynamics and transport of tropospheric source gases. *J. Geophys. Rev., 97,* 12,967-12,991, 1992.

Gillotay, D., and P.C. Simon, Ultraviolet absorption spectrum of trifluoro-bromo-methane, difluoro-dibromo-methane and difluoro-bromo-chloro-methane in the vapor phase, *J. Atmos. Chem., 8*, 41-62, 1989.

Hall, T.M. and R.A. Plumb, Age as a diagnostic of stratospheric transport, *Geophys. Res. Lett., 99*, 1059-1079, 1994.

Hall, T.M., and D.W. Waugh, The influence of nonlocal chemistry on tracer distributions: Inferring the mean age of air from SF6, *J. Geophys. Res., 103*, 13,327-13,336, 1998.

Hamill, P., and G.K. Yue, A simplified model for the production of sulfate aerosols, in *Environmental and Climatic Impact of Coal Utilization*, edited by J.J. Singh and A. Deepak, pp. 255-274, Academic, San Diego, CA, 1979.

Hanson, D.R. and A.R. Ravishankara, Heterogeneous chemistry of bromine species in sulfuric acid under stratospheric conditions, *Geophys. Res. Lett., 22,* 385-388, 1995.

Hanson, D.R., A.R. Ravishankara, and E.R. Lovejoy, Reactions of $BrONO_2$ with H_2O on submicron sulfuric acid aerosol and the implications for the lower stratosphere, *J. Geophys. Res., 101,* 9063-9069, 1996.

Harnisch, J., R. Borchers, P. Fabian, and M. Maiss, 1999: CF_4 and the age of mesospheric and polar vortex air. *Geophys. Res. Lett., 26*, 295-298.

Jackman, C.H., E.L. Fleming, S. Chandra, D.B. Considine, and J.E. Rosenfield, Past, present, and future modeled ozone trends with comparisons to observed trends, *J. Geophys. Res., 101,* 28,753-28,767, 1996.

Jacob, D.J., and M. Prather, Randon-222 as a test of convective transport in a general circulation model, *Tellus Ser. B, 42,* 118-134, 1990.

Jacob, D.J., M. Prather, S. Wofsy, and M. McElroy, Atmospheric distribution of ^{85}Kr simulated with a general circulation model, *J. Geophys. Res., 92,* 6614-6626, 1987.

Kalnay, E., et al., The NCEP/NCAR 40-year reanalysis project, *Bull. Am. Met. Soc.*, 77, 437-471, 1996.

Kasten, F., Falling speed of aerosol particles, *J. Appl. Meteorol.*, 7, 944-947, 1968.

Kawa, S.R., et al., Interpretation of NO_x/NO_y observations from AASE-II using a model of chemistry along the trajectories, *Geophys. Res. Lett., 20*, 2507-2510, 1993.

Kaye, J.A., S. Penkett, and F.M. Ormond, Report on Concentrations, Lifetimes and Trends of CFCs, Halons, and Related Species, *NASA Reference Publication 1339*, NASA Office of Mission to Planet Earth, Washington, D.C., 1994.

Kinnersley, J.S., A realistic three-component planetary wave model, with a wave-breaking parameterization. *Q.J.R. Meteor. Soc., 121,* 853-881, 1995.

Ko, M.K.W., H.R. Schneider, R.-L. Shia, D.K. Weisenstein and N.-D. Sze, A two-dimensional model with coupled dynamics, radiation, and photochemistry: 1. Simulation of the middle atmosphere. *J. Geophys. Rev., 98,* 20,429-20,440, 1993.

Ko, M.K.W., N.D. Sze, C. Scott, J.M. Rodriguez, and D.K. Weisenstein, Ozone depletion potential of CH_3Br, *J. Geophys. Res., 103,* 28187-28195, 1998.

Koike, M., Y. Kondo, H. Irie, F.J. Murcray, J. Williams, P. Fogal, R. Blatherwick, C. Camy-Payret, S. Payan, H. Oelhaf, G. Wetzel, W. Traub, D. Johnson, K. Jucks, G.C. Toon, B. Sen, J.-F. Blavier, H. Schlager, H. Ziereis, N. Toriyama, M.Y. Danilin, J.M. Rodriguez,

H. Kanzawa, and Y. Sasano, A comparison of Arctic HNO_3 profiles measured by ILAS and balloon-borne sensors, *J. Geophys. Res.*, accepted, 1999.

Kondo, Y., T. Sugita, R.J. Salawitch, M. Koike, P. Aimedieu, and T. Deshler, The effect of Pinatubo aerosols on stratospheric NO, *J. Geophys. Res., 102*, 1205-1213, 1997.

Kondo, Y., T. Sugita, M. Koike, S.R. Kawa, M.Y. Danilin, J.M. Rodriguez, S. Spreng, K. Golinger, and F. Arnold, Partitioning of reactive nitrogen in the midlatitude lower stratosphere, *J. Geophys. Res.*, accepted, 1999.

MacKay, R.M., M.K.W. Ko, S. Zhou, G. Molnar, R.-L. Shia, Y. Yang, An estimate of the climatic effect of ozone during the 1980s. *J. of Climate, 10*, 774-788, 1997.

Minschwaner, K., et al., Bulk properties of isentropic mixing into the tropics in the lower stratosphere, *J. Geophys. Res., 101,* 9433-9439, 1996.

Minschwaner, K., R. W. Carter, and B. P. Briegleb, Infrared radiative forcing and atmospheric lifetimes of trace species based on observations from UARS, submitted to *J. Geophys. Res.*, 1998.

Molina, M.J., et al., The reaction of $ClONO_2$ with HCl on aluminum oxide, *Geophys. Res. Lett., 24,* 1619-1622, 1997.

Molnar, G., M.K.W. Ko, S. Zhou and N.D. Sze, Climate consequences of the observed ozone loss in the 1980's: Relevance to the greenhouse problem, *J. Geophys. Res., 99*, 25,755-25,760, 1994.

Neu, J.L. and R.A. Plumb, Age of air in a "leaky pipe" model of stratospheric transport, *J. Geophys. Res., 104*, 19243-19255, 1999.

Oltmans, S.J. and D.J. Hofmann, Increase in lower-stratospheric water at mid-latitude Northern Hemisphere site from 1981 to 1994, *Nature, 374*, 146-149, 1995.

Park, J.H., M.K.W. Ko, R.A. Plumb, C.H. Jackman, J.A. Kaye, and K.H. Sage (eds.), Report of the Models and Measurements II, *NASA Reference Publication*, Washington, DC, 1999 (in press).

Penner, J.E., D.H. Lister, D.J. Griggs, D.J. Dokken, M. McFarland, eds., Aviation and the Global Atmosphere, A Special Report of IPCC Working Groups I and III in collaboration with the Scientific Assessment Panel to the Montreal Protocol on Substances that Deplete the Ozone Layer , published for the Intergovernmental Panel on Climate Change, Cambridge University Press, 1999.

Prather, M.J., M. McElroy, S. Wofsy, G. Russell, and D. Rind, Chemistry of global troposphere: Fluorocarbons as tracers of air motion, *J. Geophys. Res., 92,* 579-6613, 1987.

Prather, M. and E.E. Remsberg (Eds.), The atmospheric effects of stratospheric aircraft: Report of the 1992 models and measurements workshop, NASA Ref. Publ. 1292, 1993.

Randel, W.J., F. Wu, J.M. Russell III, A. Roche, and J.W. Water, Seasonal cycle and QBO variations in stratospheric CH_4 and H_2O observed in UARS HALOE Data, *J. Atoms. Sci., 55,* 163-185, 1998.

Ravishankara, A.R., S. Solomon, A.A. Turnipseed, R.F. Warren, Atmospheric lifetimes of long-lived halogenated species, *Science, 259*, 194-199, 1993.

Rinsland, C.P., M.R. Gunson, M.K.W. Ko, D.K. Weisenstein, R. Zander, M.C. Abrams, A. Goldman, N.D. Sze, and G.K. Yue, H_2SO_4 photolysis: A source of sulfur dioxide in the upper stratosphere, *Geophys. Res. Lett., 22,* 1109-1112, 1995.

Rodriguez, J.M., M.K.W. Ko, and N.D. Sze, Role of the heterogeneous conversion of N_2O_5 on sulfate aerosol in global ozone loss, *Nature, 352*, 134-137, 1991.

Schneider, H.R., M.K.W. Ko, R.-L. Shia, and N.-D. Sze, A two-dimensional model with coupled dynamics, radiative transfer, and photochemistry 2. Assessment of response of stratospheric ozone to increased levels of CO_2, N_2O, CH_4, and CFC. *J. Geophys. Res., 98,* 20,441-20,449, 1993.

Schoeberl, M.R., et al., An estimation of the dynamical isolation of the tropical lower stratosphere using UARS wind and trace gas observations of the quasi-biennial oscillation, *Geophys. Res. Lett., 24,* 53-56, 1997.

Shia, R.-L., M.K.W. Ko, D.K. Weisenstein, C. Scott and J. Rodriguez, Transport between the tropical and mid-latitude lower stratosphere: Implications for ozone response to HSCT emissions, *J. Geophys. Res., 103,* 25,435-25,446, 1998.

Shindell, D.W., et al., Increased polar stratospheric ozone losses and delayed eventual recovery owing to increasing greenhouse gas concentrations, *Nature, 392*, 589-592, 1998.

Spencer, J. E., and F. S. Rowland, Bromine Nitrate and Its Stratospheric Significance, *J. Phys. Chem.*, 82, 7-10, 1978.

Steele, H.M., and P. Hamill, Effects of temperature and humidity on the growth and optical properties of sulfuric acid-water droplets in the stratosphere, *J. Aerosol Sci., 12,* 517-528, 1981.

Tabazadeh, A., O.B. Toon, S.L. Clegg, and P. Hamill, A new parameterization of H_2SO_4/H_2O aerosol composition: Atmospheric implications, *Geophys. Res. Lett., 24,* 1931-1934, 1997.

Volk, C.M., et al., Quantifying transport between the tropical and mid-latitude lower stratosphere, *Science, 272,* 1763-1768, 1996.

Volk, C.M., J. W. Elkins, D.W. Fahey, G.S. Dutton, J.M. Gilligan, M. Loewenstein, J.R. Podolske, K.R. Chan, and M.R. Gunson, Evaluation of source gas lifetimes from stratospheric observations, *J. Geophys. Res., 102,* 25,543-25,564, 1997.

Weisenstein, D.K., M.K.W. Ko, N.-D. Sze, and J.M. Rodriguez, Potential impact of SO_2 emissions from stratospheric aircraft on ozone, *Geophys. Res. Lett., 23,* 161-164, 1996.

Weisenstein, D.K., G.K. Yue, M.K.W. Ko, N.D. Sze, J.M. Rodriguez, and C.J. Scott, A two-dimensional model of sulfur species and aerosol, *J. Geophys. Res., 102,* 13,019-13,035, 1997.

Weisenstein, D.K., et al., HSCT assessment calculations with the AER 2-D model: Sensitivities to transport formulation, PSC formulation, interannual temperature variation, presented at NASA Atmospheric Effects of Aviation Annual Meeting, Virginia Beach, VA, April 27-May 1, 1998.

Wennberg, P.O., et al., Removal of stratospheric O_3 by radicals: in situ measurements of OH, HO_2, NO, NO_2, ClO, and BrO, *Science, 266*, 398-404, 1994.

WMO, Scientific Assessment of Ozone Depletion: 1994, Rep. 37, Geneva, 1995.

WMO, Scientific Assessment of Ozone Depletion: 1998, Rep. 44, Geneva, 1999.

Yue, G.K. and A. Deepak, Modeling of coagulation-sedimentation effects on transmission of visible IR laser beams in aerosol media, *Appl. Opt., 18,* 3918-3925, 1979.

Yue, G.K. and A. Deepak, Temperature dependence of the formation of sulfate aerosols in the stratosphere, *J. Geophys. Res., 87,* 3128-3134, 1982.

Zhao, J. and R.P. Turco, Nucleation simulations in the wake of a jet aircraft in stratospheric flight, *J. Aerosol Sci.*, 26, 779-795, 1995.